Certain computational aspects of vector diffraction problems

M. Mansuripur

Optical Sciences Center, University of Arizona, Tucson, Arizona 85721

Received July 6, 1988; accepted December 20, 1988

Fourier decomposition of a given amplitude distribution into plane waves and the subsequent superposition of these waves after propagation is a powerful yet simple approach to diffraction problems. Many vector diffraction problems can be formulated in this way, and the classical results are usually the consequence of a stationary-phase approximation to the resulting integrals. For situations in which the approximation does not apply, a factorization technique is developed that substantially reduces the required computational resources. Numerical computations are based on the fast-Fourier-transform algorithm, and the practicality of this method is shown with several examples.

1. INTRODUCTION

A. Background

The essence of diffraction theory is Huygens's principle, which states that every point on a given wave front can be treated as a source of radiation, emanating spherical wavelets that can be superimposed later to yield the light-amplitude distribution. A slight variation on this theme is the view that the wave front can be decomposed into a set of plane waves that propagate independently through space and that their superposition is the field at any given point.[1–4] The two views can be shown to be identical and to lead to the same results, although the latter approach is mathematically more convenient. The Fourier-transform technique is the natural vehicle for decomposition into and superposition of plane waves, and, in fact, the majority of problems in the classical theory of diffraction can be reduced to a pair of Fourier- and inverse Fourier-transform integrals. The trouble, from a computational point of view, is that usually the functions involved in these transformations are highly oscillatory and consequently require a large number of samples for proper representation. It turns out, however, that in many problems of practical interest one or the other of the Fourier integrals can be approximated quite accurately with the stationary-phase technique.[5,6] For instance, in the problem of far-field (Fraunhofer) diffraction from an aperture, the stationary-phase approximation applies to the second (superposition) integral, whereas in the case of diffraction from a lens the approximation is used to eliminate the first (decomposition) integral. In both cases the remaining integral can then be computed efficiently with the fast-Fourier-transform (FFT) algorithm.

Like any approximation, the stationary-phase technique is valid only over a certain range of the parameters involved. When the parameter set happens to be outside the proper range, one goes back to evaluate the original Fourier integrals more accurately. Near-field (Fresnel) diffraction from an aperture is but one representative of problems in which the stationary-phase approximation fails. Another example is diffraction from a lens with a small numerical aperture. It is well-known that at small numerical apertures the distribution becomes asymmetric with respect to the focal point and the maximum intensity occurs at a point that is somewhat closer to the lens than the point of geometric focus.[7–9] This contrasts sharply with the prediction of symmetry by theories that are based on the stationary-phase approximation.[2]

In this paper a factorization technique is presented that enables one to compute the Fourier integrals of diffraction theory more efficiently. The price of the reduction in the required number of samples (made possible by factorization) is an extra Fourier transform: instead of transforming a large array twice, one must now transform a smaller array three times. The obvious advantage of factorization is therefore the reduced level of computational resources (memory and CPU time) that a given problem requires. It is important to emphasize that factorization does not eliminate the need for the stationary-phase approximation (wherever it legitimately applies), nor does it further simplify problems in which the original Fourier and inverse Fourier integrals are readily computable. Simply stated, the factorization technique covers the gray boundary area between these two regions, where approximation is inaccurate and direct computation is costly.

The organization of the paper is as follows. In the remainder of this section the notation is introduced, and the background is provided for the problem formulation. In Section 2, we discuss the basic equations of vector diffraction theory and describe the factorization technique in detail. In Section 3 factorization is applied to problems of diffraction in the presence of a lens. The important case of a spherical lens is treated in detail in Subsections 3.A and 3.B, and the (rather exotic) cases of an astigmatic lens and a ring lens are treated in Subsections 3.C–3.E. In Section 4 the results are given for numerical computations based on the various methods described in this paper. The results are intended to give an appreciation for the range of applicability of each technique.

B. Preliminaries

The notation and some elementary aspects of the formalism used throughout the paper are as follows[10]:

1. $t(x, y)$ is a two-dimensional function defined on the xy

plane. When the x axis is normalized by a and the y axis is normalized by b, we define new coordinates $\mathbf{x}$ and $\mathbf{y}$, such that $x = a\mathbf{x}$ and $y = b\mathbf{y}$, and represent the function in this new coordinate system as $t(a\mathbf{x}, b\mathbf{y})$.

2. The Fourier transform of $t(x, y)$ is $T(u, v)$ and is written

$$T(u, v) = \mathcal{F}\{t(x, y)\} = \int\int_{-\infty}^{\infty} t(x, y)\exp[-i2\pi(xu + yv)]\mathrm{d}x\mathrm{d}y. \tag{1.1}$$

If x and y are normalized by a and b, respectively, the Fourier transform of the scaled function is

$$\frac{1}{ab} T\left(\frac{u}{a}, \frac{v}{b}\right) = \mathcal{F}\{t(a\mathbf{x}, b\mathbf{y})\} = \int\int_{-\infty}^{\infty} t(a\mathbf{x}, b\mathbf{y}) \times \exp[-i2\pi(\mathbf{x}u + \mathbf{y}v)]\mathrm{d}\mathbf{x}\mathrm{d}\mathbf{y}. \tag{1.2}$$

3. The inverse transform of $T(u, v)$ is $t(x, y)$ as follows:

$$t(x, y) = \mathcal{F}^{-1}\{T(u, v)\} = \int\int_{-\infty}^{\infty} T(u, v)\exp[i2\pi(xu + yv)]\mathrm{d}u\mathrm{d}v. \tag{1.3}$$

4. The discrete array used for numerical computations is initially in the $\mathbf{xy}$ plane, where $\mathbf{x} = x/\lambda$ and $\mathbf{y} = y/\lambda$ are dimensionless coordinates; i.e., $\mathbf{x}$ and $\mathbf{y}$ are in units of the wavelength λ. The length of the array in the $\mathbf{x}$ direction is $L_{\max}$, and the number of pixels in this dimension is $N_{\max}$. The corresponding parameters along the $\mathbf{y}$ axis are L_{may} and N_{may}. Because the arrays are transformed by the FFT algorithm, it is preferable that $N_{\max}$ and N_{may} be powers of 2. The array generally is centered at the origin, and the (I, J) pixel represents the point $\mathbf{x} = (I - N_{\mathrm{midx}} - 1)L_{\max}/N_{\max}$, $\mathbf{y} = (J - N_{\mathrm{midy}} - 1)L_{\mathrm{may}}/N_{\mathrm{may}}$, where $N_{\mathrm{midx}} = N_{\max}/2$ and $N_{\mathrm{midy}} = N_{\mathrm{may}}/2$. The spacing between nearest-neighbor pixels is $\Delta_x = L_{\max}/N_{\max}$ and $\Delta_y = L_{\mathrm{may}}/N_{\mathrm{may}}$. For the most part in this paper we have square lattices with $L_{\mathrm{may}} = L_{\max}$, $N_{\mathrm{may}} = N_{\max}$, and $\Delta_y = \Delta_x$. Thus, when there is no danger of confusion, we shall express the relationships in terms of $L_{\max}$, $N_{\max}$, and Δ, with the understanding that similar relationships exist for the $\mathbf{y}$ direction.

5. To normalize the x axis by a we divide $L_{\max}$ by a. Thus, if $t(x, y)$ is represented by an $N_{\max} \times N_{\mathrm{may}}$ array on an $L_{\max} \times L_{\mathrm{may}}$ rectangle, its scaled version $t(a\mathbf{x}, b\mathbf{y})$ has the same pixels but is on a rectangle of dimensions $(L_{\max}/a) \times (L_{\mathrm{may}}/b)$.

6. The discrete Fourier transform of an $L_{\max} \times L_{\mathrm{may}}$ array with $N_{\max} \times N_{\mathrm{may}}$ pixels is another array with the same number of pixels but with new dimensions $\tilde{L}_{\max} \times \tilde{L}_{\mathrm{may}}$. In general, $\tilde{L}_{\max} = N_{\max}/L_{\max}$ and $\tilde{L}_{\mathrm{may}} = N_{\mathrm{may}}/L_{\mathrm{may}}$.

7. When a linearly polarized plane wave traveling along the z axis encounters a prism, as shown in Fig. 1, its direction of propagation changes to $\hat{\sigma} = (\sigma_x, \sigma_y, \sigma_z)$. The effect of refraction on the polarization vector is to keep the S component unchanged but to reorient the P component such that it becomes perpendicular to $\hat{\sigma}$. The new polarization components Ψ_x, Ψ_y, and Ψ_z can thus be calculated for any incident polarization by simple geometric considerations. Table 1 shows the results for x-polarized (top three rows) and y-polarized (bottom three rows) incident beams. Notice that $\hat{\sigma}$ is a unit vector and thus that $\sigma_z = (1 - \sigma_x^2 - \sigma_y^2)^{1/2}$.

8. A coherent point source located at the origin gives rise to a spherical wave front. The amplitude distribution in a

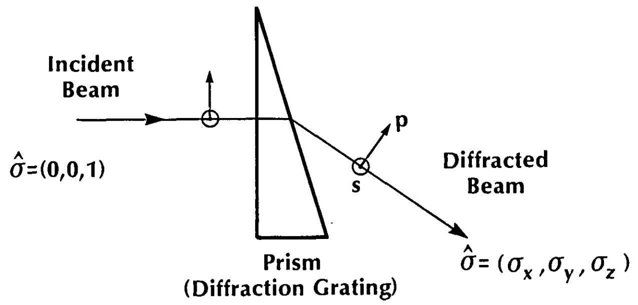

Fig. 1. Prism as a diffraction grating. A plane, linearly polarized incident beam is diffracted into a plane wave propagating along $\hat{\sigma} = (\sigma_x, \sigma_y, \sigma_z)$. The relationship between the incident and the diffracted polarizations is summarized in Table 1.

Table 1. Components of the Polarization Vector of a Plane Wave[a] Propagating along the Unit Vector $\hat{\sigma} = (\sigma_x, \sigma_y, \sigma_z)$

Component	Expression
Ψ_{yx}	$-\frac{\sigma_x\sigma_y}{1+\sigma_z}$
Ψ_{yy}	$1-\frac{\sigma_y^2}{1+\sigma_z}$
Ψ_{yz}	$-\sigma_y$
Ψ_{xx}	$1-\frac{\sigma_x^2}{1+\sigma_z}$
Ψ_{xy}	$-\frac{\sigma_x\sigma_y}{1+\sigma_z}$
Ψ_{xz}	$-\sigma_x$

[a] The beam is obtained by the refraction (through a properly oriented prism) of a linearly polarized wave propagating along $\hat{\sigma}_0 = (0, 0, 1)$. $\Psi_{\alpha\beta}$ is the β component of the refracted beam when the (unit-amplitude) incident beam is polarized along α.

plane perpendicular to the positive z axis is said to have a curvature $C = 1/z$. The curvature phase factor is given by

$$A(x, y) = \exp\left\{i\frac{2\pi}{\lambda C}[1 + C^2(x^2 + y^2)]^{1/2}\right\}. \tag{1.4}$$

If the coordinates are normalized by the wavelength such that $\mathbf{x} = x/\lambda$, $\mathbf{y} = y/\lambda$, and $\mathbf{z} = z/\lambda$, then we define the normalized curvature $\mathbf{C} = \lambda C$ in order to eliminate λ from Eq. (1.4). In this notation a positive curvature represents a diverging beam centered to the left of the xy plane, and a negative curvature corresponds to a converging beam toward a point to the right of the xy plane.

2. PROPAGATION IN FREE SPACE

A. Direct Application of Fresnel's Formula

It is well known that an amplitude distribution $t(x, y)$ in the xy plane can be considered the superposition of plane waves propagating along the unit vectors $\hat{\sigma} = [\sigma_x, \sigma_y, (1 - \sigma_x^2 - \sigma_y^2)^{1/2}]$. The complex amplitude of each plane wave is related to the Fourier transform of $t(x, y)$ as follows[1]:

$$\lambda^{-2}T\left(\frac{\sigma_x}{\lambda}, \frac{\sigma_y}{\lambda}\right) = \begin{cases}\mathcal{F}\{t(\lambda\mathbf{x}, \lambda\mathbf{y})\} & \sigma_x^2 + \sigma_y^2 \le 1 \\ 0 & \text{otherwise}\end{cases}. \tag{2.1}$$

Here $x = \lambda\mathbf{x}$, $y = \lambda\mathbf{y}$, and $\mathcal{F}\{\cdot\}$ is the two-dimensional Fourier-transform operator.

At a distance z from the origin the distribution is the superposition of the above plane waves, each multiplied by a proper phase factor in order to represent different propagation distances. Let us assume that each plane wave originates at the $z = 0$ plane by going through a properly oriented prism; then, if the incident beam is polarized along the α axis (α is either x or y), the contribution of the wave traveling along $\hat{\sigma}$ to the final polarization along β (β is x or y or z) will be $\Psi_{\alpha\beta}(\sigma_x, \sigma_y)$ as given in Table 1. Thus the amplitude distribution of β-polarized light at $z = \lambda\mathbf{z}$ is[10]

$$\tilde{t}_{\alpha\beta}(\lambda\mathbf{x}, \lambda\mathbf{y}, \lambda\mathbf{z}) = \mathcal{F}^{-1}\left\{\lambda^{-2}T\left(\frac{\sigma_x}{\lambda}, \frac{\sigma_y}{\lambda}\right)\Psi_{\alpha\beta}(\sigma_x, \sigma_y) \times \exp[i2\pi\mathbf{z}(1 - \sigma_x{}^2 - \sigma_y{}^2)^{1/2}]\right\}. \quad (2.2)$$

The Fourier-transform pair of Eqs. (2.1) and (2.2) constitutes the basic formula for propagation in the Fresnel regime. For numerical computations one needs a two-dimensional array to represent the initial and final distributions, as well as the intermediate functions. Let the linear dimension of this array (after normalization by λ) be $L_{\max}$, and let $N_{\max}$ represent the number of samples (pixels) in this dimension. The sample spacing Δ must be small enough in order to represent properly the fine features of $t(\lambda\mathbf{x}, \lambda\mathbf{y})$. For instance, if the incident beam is uniform within a circular aperture of radius $R = \lambda\mathbf{R}$, then $\Delta \le \mathbf{R}/10$ is an appropriate choice. On the other hand, if the incident beam has a curvature $\mathbf{C}$, as in Eq. (1.4), then the fastest oscillations of the phase factor occur in the vicinity of the aperture edge, where the radial spacing between successive peaks (or valleys) is $\sim(1 + \mathbf{C}^2\mathbf{R}^2)^{1/2}/|\mathbf{C}|\mathbf{R}$. Consequently, Δ must satisfy the restriction

$$\Delta \le \min\left\{\frac{\mathbf{R}}{10}, \frac{(1 + \mathbf{C}^2\mathbf{R}^2)^{1/2}}{2|\mathbf{C}|\mathbf{R}}\right\}. \quad (2.3)$$

After the first transformation, the spacing between nearest-neighbor elements becomes $\tilde{\Delta} = 1/L_{\max}$. The proper choice of $\tilde{\Delta}$ now depends on the functions that appear on the right-hand side of Eq. (2.2). The smallest features of $\lambda^{-2}T(\sigma_x/\lambda, \sigma_y/\lambda)$ in the $\sigma_x\sigma_y$ plane occur on a scale of $(R/\lambda)^{-1}$, where as before, R is the largest linear dimension of the aperture distribution $t(x, y)$. Thus $\tilde{\Delta} \le (10\mathbf{R})^{-1}$ is a good choice as far as $T(\sigma_x/\lambda, \sigma_y/\lambda)$ is concerned. The second function, $\Psi_{\alpha\beta}(\sigma_x, \sigma_y)$, is relatively smooth, and we need not be concerned about it at this point. The third function is an exponential phase factor that oscillates with increasing frequency as one moves away from the origin in the $\sigma_x\sigma_y$ plane. At a distance $\sigma_{\max}$ from the origin, the radial separation between successive peaks of this function is $\sim(1 - \sigma_{\max}^2)^{1/2}/(\mathbf{z}\sigma_{\max})$. Consequently, $\tilde{\Delta}$ must be small enough to sample these oscillations properly. $\sigma_{\max}$ itself depends on the spatial variations of $t(x, y)$; in fact, it is the largest spatial frequency contained in $t(\lambda\mathbf{x}, \lambda\mathbf{y})$. For the preceding example,

$$\sigma_{\max} = \frac{|\mathbf{C}|\mathbf{R}}{(1 + \mathbf{C}^2\mathbf{R}^2)^{1/2}} + \frac{1}{2\mathbf{R}}. \quad (2.4)$$

Since $\tilde{\Delta}$ is the inverse of $L_{\max}$, these considerations yield

$$L_{\max} \ge \max\left\{10\mathbf{R}, \frac{2\mathbf{z}\sigma_{\max}}{(1 - \sigma_{\max}^2)^{1/2}}\right\}. \quad (2.5)$$

Relations (2.3) and (2.5) and Eq. (2.4) may be used for selecting $L_{\max}$ and $N_{\max}$ for numerical computations. Relation (2.5) is general and applies to all cases of Fresnel propagation, whereas relation (2.3) and Eq. (2.4) correspond to apertures illuminated with spherical waves only.

B. Extending the Range of Fresnel's Formula

As can be seen from relation (2.5), when the spatial variations of $t(\lambda\mathbf{x}, \lambda\mathbf{y})$ are rapid, (i.e., when $\sigma_{\max}$ is large) and/or when $\mathbf{z}$ is large, numerical computations may become impractical. One way around the problem is to separate the oscillating terms from Eq. (2.2). To this end, we define $G(\sigma_x, \sigma_y)$ as

$$G(\sigma_x, \sigma_y) = \lambda^{-2}T(\sigma_x/\lambda, \sigma_y/\lambda)\Psi_{\alpha\beta}(\sigma_x, \sigma_y) \times \exp\{i2\pi\mathbf{z}[(1 - \sigma_x{}^2 - \sigma_y{}^2)^{1/2} + \tfrac{1}{2}\eta(\sigma_x{}^2 + \sigma_y{}^2)]\} \quad (2.6)$$

and rewrite Eq. (2.2) as

$$\tilde{t}_{\alpha\beta}(\lambda\mathbf{x}, \lambda\mathbf{y}, \lambda\mathbf{z}) = \mathcal{F}^{-1}\{G(\sigma_x, \sigma_y)\exp[-i\pi\eta\mathbf{z}(\sigma_x{}^2 + \sigma_y{}^2)]\}. \quad (2.7)$$

Here η is a parameter that can be optimized to reduce the oscillations of the phase factor in Eq. (2.6). A method of finding the optimum η is given in Appendix A. Since the inverse transform of the product of two functions is the convolution of individual inverse transforms, Eq. (2.7) is written

$$\tilde{t}_{\alpha\beta}(\lambda\mathbf{x}, \lambda\mathbf{y}, \lambda\mathbf{z}) = \iint_{-\infty}^{\infty} \mathcal{F}^{-1}\{G(\sigma_x, \sigma_y)\}\left(\frac{-i}{\eta\mathbf{z}}\right) \times \exp\left\{\frac{i\pi}{\eta\mathbf{z}}[(\mathbf{x} - \mathbf{x}')^2 + (\mathbf{y} - \mathbf{y}')^2]\right\}\mathrm{d}\mathbf{x}'\mathrm{d}\mathbf{y}'. \quad (2.8)$$

Let us define $H(\mathbf{x}, \mathbf{y})$ as follows:

$$H(\mathbf{x}, \mathbf{y}) = -i\eta\mathbf{z}\exp\left[\frac{i\pi}{\eta\mathbf{z}}(\mathbf{x}^2 + \mathbf{y}^2)\right]\mathcal{F}^{-1}\{G(\sigma_x, \sigma_y)\}; \quad (2.9)$$

then, when the normalized variables $X = \mathbf{x}/\eta\mathbf{z}$ and $Y = \mathbf{y}/\eta\mathbf{z}$ are used, Eq. (2.8) becomes

$$\tilde{t}_{\alpha\beta}(\lambda\mathbf{x}, \lambda\mathbf{y}, \lambda\mathbf{z}) = \exp\left[\frac{i\pi}{\eta\mathbf{z}}(\mathbf{x}^2 + \mathbf{y}^2)\right]\mathcal{F}\{H(\eta\mathbf{z}X, \eta\mathbf{z}Y)\}. \quad (2.10)$$

We summarize the results by outlining the steps in the computation of Fresnel propagation with an extended range:

1. Calculate $\lambda^{-2}T(\sigma_x/\lambda, \sigma_y/\lambda)$ from Eq. (2.1). As before, the sample spacing Δ depends on the spatial variations of $t(\lambda\mathbf{x}, \lambda\mathbf{y})$, and, for the simple example of an aperture with a spherical incident wave front, it is given by relation (2.3).
2. Calculate $G(\sigma_x, \sigma_y)$ from Eq. (2.6). The spacing $\tilde{\Delta}$ in the $\sigma_x\sigma_y$ plane is the inverse of $L_{\max}$. To choose the correct $L_{\max}$, one needs to know the maximum frequency $\sigma_{\max}$ of the input distribution. [$\sigma_{\max}$ for the case of an aperture with a spherical incident wave front is given in Eq. (2.4).] Once $\sigma_{\max}$ is determined, one calculates η_{opt} and $\hat{\omega}_{\max}$ by using the procedure outlined in Appendix A. The same considerations that led to relation (2.5) now yield

$$L_{\max} \geq \max\{10\mathbf{R}, 2\mathbf{z}\dot{\omega}_{\max}\}. \tag{2.11}$$

3. Calculate $H(\mathbf{x}, \mathbf{y})$ from Eq. (2.9). The largest distance from the origin of the $\mathbf{xy}$ plane that is now significant is $\mathbf{R} + \mathbf{z}\dot{\omega}_{\max}$. At this distance the separation between successive peaks of the exponential phase factor in Eq. (2.9) poses another restriction on Δ as follows:

$$\Delta \leq \frac{\eta \mathbf{z}}{2(\mathbf{R} + \mathbf{z}\dot{\omega}_{\max})}. \tag{2.12}$$

Note that Eq. (2.12) must be satisfied in addition to Eq. (2.3).

4. Normalize the axes $\mathbf{xy}$ of the domain of $H(\mathbf{x}, \mathbf{y})$ in order to obtain $H(\eta \mathbf{z}X, \eta \mathbf{z}Y)$. This is done simply by dividing $L_{\max}$ and L_{may} by $\eta\mathbf{z}$.

5. Calculate the final distribution according to Eq. (2.10). The separation between neighboring elements in the final array is $\tilde{\Delta} = \eta\mathbf{z}/L_{\max}$ because of the normalization in the preceding step. The length of the final array is thus

$$\tilde{L}_{\max} = \eta \mathbf{z} N_{\max}/L_{\max}. \tag{2.13}$$

The phase factor in Eq. (2.10) may be treated as a curvature $\mathbf{C} = (\eta\mathbf{z})^{-1}$, provided that $\mathbf{C}$ is sufficiently small.

C. Fresnel's Formula and the Stationary-Phase Approximation

When $\mathbf{z}$ is sufficiently large, the inverse transform in Eq. (2.2) can be evaluated with the stationary-phase approximation. The exponent of the integrand is

$$W(\sigma_x, \sigma_y) = \mathbf{x}\sigma_x + \mathbf{y}\sigma_y + \mathbf{z}(1 - \sigma_x^2 - \sigma_y^2)^{1/2}, \tag{2.14}$$

which has a stationary point at

$$\sigma_{x0} = \mathbf{x}/(\mathbf{x}^2 + \mathbf{y}^2 + \mathbf{z}^2)^{1/2}, \tag{2.15a}$$

$$\sigma_{y0} = \mathbf{y}/(\mathbf{x}^2 + \mathbf{y}^2 + \mathbf{z}^2)^{1/2}. \tag{2.15b}$$

The Taylor-series expansion of $W(\sigma_x, \sigma_y)$ around the stationary point is

$$\begin{aligned} W(\sigma_x, \sigma_y) = (\mathbf{x}^2 + \mathbf{y}^2 + \mathbf{z}^2)^{1/2}\{&1 - \tfrac{1}{2}[1 + (\mathbf{x}/\mathbf{z})^2](\sigma_x - \sigma_{x0})^2 \\ &- (\mathbf{xy}/\mathbf{z}^2)(\sigma_x - \sigma_{x0})(\sigma_y - \sigma_{y0}) \\ &- \tfrac{1}{2}[1 + (\mathbf{y}/\mathbf{z})^2](\sigma_y - \sigma_{y0})^2\} + \ldots. \end{aligned} \tag{2.16}$$

After replacing $W(\sigma_x, \sigma_y)$ in Eq. (2.2) and completing the stationary-phase method, one obtains

$$\tilde{t}_{\alpha\beta}(\lambda\mathbf{x}, \lambda\mathbf{y}, \lambda\mathbf{z}) = -(i/\mathbf{z})\exp\left[i2\pi\mathbf{z}\left(1 + \frac{\mathbf{x}^2 + \mathbf{y}^2}{\mathbf{z}^2}\right)^{1/2}\right] \times \Psi_{\alpha\beta}(\sigma_{x0}, \sigma_{y0})(1 - \sigma_{x0}^2 - \sigma_{y0}^2)[\lambda^{-2}T(\sigma_{x0}/\lambda, \sigma_{y0}/\lambda)], \tag{2.17}$$

which is the standard expression for the far-field (Fraunhofer) diffraction.[11] Note that the exponential term is a curvature phase factor with a radius of curvature $\mathbf{z}$.

For numerical computations the sampling interval must be sufficiently small to represent the fine features of the incident waveform. The restriction on Δ is thus similar to that for the direct Fresnel method, and, when the aperture radius is $\mathbf{R}$ and the incident beam has a curvature $\mathbf{C}$, the upper limit of Δ is given by relation (2.3). The lower bound on $L_{\max}$, however, is different here; the only requirement is for sufficient resolution in the output plane, namely,

$$L_{\max} \geq 10\mathbf{R}. \tag{2.18}$$

Since σ_{x0} and σ_{y0} are the angular coordinates of the observation point $(\mathbf{x}, \mathbf{y}, \mathbf{z})$, a nonlinear scaling must be applied to the function in Eq. (2.17). The final array dimension is

$$\tilde{L}_{\max} = \frac{\mathbf{z} \cdot N_{\max}}{L_{\max}}. \tag{2.19}$$

3. DIFFRACTION IN THE PRESENCE OF A LENS

A. Spherical Lens

Consider a spherical lens with a focal length f and a numerical aperture NA. Let the lens center be located at (x_c, y_c), and let the amplitude distribution in the plane of the entrance pupil be $\tau_0(x, y)$. The distribution at the exit pupil is then

$$t(x, y) = \tilde{\tau}_0(x, y)\exp\left\{-i\frac{2\pi}{\lambda}[f^2 + (x - x_c)^2 + (y - y_c)^2]^{1/2}\right\}. \tag{3.1a}$$

$\tilde{\tau}_0(x, y)$ is a scaled version of $\tau_0(x, y)$ as follows:

$$\tilde{\tau}_0(x, y) = \tau_0\left\{\frac{x - x_c}{\left[1 + \left(\frac{x - x_c}{f}\right)^2 + \left(\frac{y - y_c}{f}\right)^2\right]^{1/2}} + x_c, \frac{y - y_c}{\left[1 + \left(\frac{x - x_c}{f}\right)^2 + \left(\frac{y - y_c}{f}\right)^2\right]^{1/2}} + y_c\right\} \times \left[1 + \left(\frac{x - x_c}{f}\right)^2 + \left(\frac{y - y_c}{f}\right)^2\right]^{-1}. \tag{3.1b}$$

The scaling is in keeping with Abbe's sine condition for an aplanatic lens.[5] In addition, $\tilde{\tau}_0(x, y)$ may include any aberrations introduced into the beam while it is traveling between the entrance and the exit pupils.

Although the distribution in Eq. (3.1) can be propagated by using Fresnel's formula, the oscillatory nature of the phase factor at high numerical apertures will require a large number of samples. To avoid this problem, a factorization similar to that used in Section 2 is proposed. Here we define the function $\tau(x, y)$ as follows:

$$\tau(x, y) = \begin{cases} \tilde{\tau}_0(x, y)\exp\left(-i\dfrac{2\pi f}{\lambda}\left\{\left[1 + \dfrac{(x - x_c)^2 + (y - y_c)^2}{f^2}\right]^{1/2} - \dfrac{1}{2}\eta\dfrac{(x - x_c)^2 + (y - y_c)^2}{f^2}\right\}\right). \\ 0 \qquad [(x - x_c)^2 + (y - y_c)^2]^{1/2} > f\tan[\arcsin(\mathrm{NA})] \end{cases} \tag{3.2}$$

In this equation η is a parameter that can be optimized for a minimum number of samples in the xy plane. Equation (3.1a) then becomes

$$t(x, y) = \tau(x, y)\exp\left\{-i\frac{\pi\eta}{\lambda f}[(x - x_c)^2 + (y - y_c)^2]\right\}. \tag{3.3}$$

Let us now define $\mathbf{f} = f/\lambda$, $X_c = \eta x_c/f$, $Y_c = \eta y_c/f$, $X = \eta x/f$, and $Y = \eta y/f$; then Eqs. (3.2) and (3.3) are written

$$\tau\left(\frac{f}{\eta}X, \frac{f}{\eta}Y\right) = \tilde{\tau}_0\left(\frac{f}{\eta}X, \frac{f}{\eta}Y\right)\exp\left(-i2\pi\mathbf{f}\times\left\{\left[1 + \frac{(X - X_c)^2 + (Y - Y_c)^2}{\eta^2}\right]^{1/2} - \frac{1}{2}\frac{(X - X_c)^2 + (Y - Y_c)^2}{\eta}\right\}\right), \tag{3.4}$$

$$t\left(\frac{f}{\eta}X, \frac{f}{\eta}Y\right) = \tau\left(\frac{f}{\eta}X, \frac{f}{\eta}Y\right)\times\exp\left\{\frac{-i\pi\mathbf{f}}{\eta}[(X - X_c)^2 + (Y - Y_c)^2]\right\}. \tag{3.5}$$

The first step in propagating the distribution in Eq. (3.5) beyond the lens is finding its Fourier transform according to Eq. (2.1). However, Eq. (3.5) is the product of two functions, and its Fourier transform is consequently a convolution as follows:

$$\left(\frac{\eta}{f}\right)^2 T\left(\frac{\eta u}{f}, \frac{\eta v}{f}\right) = -\frac{i\eta}{\mathbf{f}}\int\int_{-\infty}^{\infty}\mathcal{F}\left\{\tau\left(\frac{f}{\eta}X, \frac{f}{\eta}Y\right)\right\}\times\exp\{-i2\pi[X_c(u - u') + Y_c(v - v')]\}\times\exp\left\{\frac{i\pi\eta}{\mathbf{f}}[(u - u')^2 + (v - v')^2]\right\}\mathrm{d}u'\mathrm{d}v'. \tag{3.6}$$

Let $\sigma_x = \eta u/\mathbf{f}$ and $\sigma_y = \eta v/\mathbf{f}$ and rewrite Eq. (3.6) as follows:

$$\lambda^{-2}T\left(\frac{\sigma_x}{\lambda}, \frac{\sigma_y}{\lambda}\right) = -\frac{i\mathbf{f}}{\eta}\exp\left[\frac{i\pi\mathbf{f}}{\eta}(\sigma_x^2 + \sigma_y^2) - i\frac{2\pi}{\lambda}(x_c\sigma_x + y_c\sigma_y)\right]\times\int\int_{-\infty}^{\infty}\mathcal{F}\left\{\tau\left(\frac{f}{\eta}X, \frac{f}{\eta}Y\right)\right\}\times\exp\left\{\frac{i\pi\eta}{\mathbf{f}}\left[\left(u' + \frac{x_c}{\lambda}\right)^2 + \left(v' + \frac{y_c}{\lambda}\right)^2\right]\right\}\times\exp[-i2\pi(u'\sigma_x + v'\sigma_y)]\mathrm{d}u'\mathrm{d}v'. \tag{3.7}$$

Again, let $\mathbf{x}_c = x_c/\lambda$ and $\mathbf{y}_c = y_c/\lambda$, and define $h(u, v)$ as

$$h(u, v) = -\frac{i\mathbf{f}}{\eta}\exp\left\{\frac{i\pi\eta}{\mathbf{f}}[(u + \mathbf{x}_c)^2 + (v + \mathbf{y}_c)^2]\right\}\times\mathcal{F}\left\{\tau\left(\frac{\lambda\mathbf{f}}{\eta}X, \frac{\lambda\mathbf{f}}{\eta}Y\right)\right\}; \tag{3.8}$$

then Eq. (3.7) becomes

$$\lambda^{-2}T\left(\frac{\sigma_x}{\lambda}, \frac{\sigma_y}{\lambda}\right) = \exp\left\{i2\pi\left[\frac{\mathbf{f}}{2\eta}(\sigma_x^2 + \sigma_y^2) - \mathbf{x}_c\sigma_x - \mathbf{y}_c\sigma_y\right]\right\}\times\mathcal{F}\{h(u, v)\}. \tag{3.9}$$

When Eq. (3.9) is substituted into Eq. (2.2) and $g(\sigma_x, \sigma_y)$ is defined as

$$g(\sigma_x, \sigma_y) = \exp[i2\pi(\mathbf{z} - \mathbf{f})(1 - \sigma_x^2 - \sigma_y^2)^{1/2}\times\exp\left\{i2\pi\mathbf{f}\left[(1 - \sigma_x^2 - \sigma_y^2)^{1/2} + \frac{1}{2\eta}(\sigma_x^2 + \sigma_y^2)\right]\right\}\times\exp[-i2\pi(\mathbf{x}_c\sigma_x + \mathbf{y}_c\sigma_y)]\mathcal{F}\{h(u, v)\}, \tag{3.10}$$

the final distribution can be written as

$$\tilde{t}_{\alpha\beta}(\lambda\mathbf{x}, \lambda\mathbf{y}, \lambda\mathbf{z}) = \mathcal{F}^{-1}\{\Psi_{\alpha\beta}(\sigma_x, \sigma_y)g(\sigma_x, \sigma_y)\}. \tag{3.11}$$

We summarize the results of this section in the following step-by-step method of calculating diffraction patterns for a lens:

1. Compute $\tau(x, y)$ from Eq. (3.2). The optimum η is obtained by the method described in Appendix B with $\theta_1 = 0$ and $\theta_2 = \arcsin(\mathrm{NA})$. Since the maximum spatial frequency of the exponential phase factor in Eq. (3.2) is $\dot{\omega}_{\max}$, the restriction on the sample spacing Δ at the aperture is

$$\Delta \le \min\left\{\frac{\mathbf{R}}{10}, \frac{1}{2\dot{\omega}_{\max}}\right\}. \tag{3.12}$$

Here $\mathbf{R} = \mathbf{f}\tan[\arcsin(\mathrm{NA})]$, and $\dot{\omega}_{\max}$, a function of NA, is given in Fig. 18 of Appendix B.

2. Normalize the coordinates $\mathbf{xy}$ by dividing $L_{\max}$ and L_{may} by $\mathbf{f}/\eta$; then calculate the Fourier transform of $\tau(x, y)$ in the new (normalized) coordinates XY. Multiply the result by the appropriate coefficient as in Eq. (3.8) to obtain $h(u, v)$. The extent of the function $h(u, v)$ in the uv plane is

$$\sigma_{\max} = \frac{\mathbf{f}}{\eta}\left(\dot{\omega}_{\max} + \frac{1}{2\mathbf{R}}\right). \tag{3.13}$$

The phase factor in Eq. (3.8) has a maximum frequency of $(\sigma_{\max} + \mathbf{r}_c)\eta/\mathbf{f}$, where $r_c = (x_c^2 + y_c^2)^{1/2}$ is the radial distance of the lens center from the optical axis. Thus $\eta L_{\max}/\mathbf{f}$ (the normalized $L_{\max}$ of the XY domain) must be greater than twice this frequency, namely,

$$L_{\max} \ge \max\left\{10\mathbf{R}, \frac{2\mathbf{f}}{\eta}\left(\dot{\omega}_{\max} + \frac{1}{2\mathbf{R}}\right) + 2\mathbf{r}_c\right\}. \tag{3.14}$$

3. Calculate $g(\sigma_x, \sigma_y)$ from Eq. (3.10). It turns out that $\dot{\omega}_{\max}$ in Appendixes A and B at optimum η are related by $\dot{\omega}_{\max}{}^{(A)} = \dot{\omega}_{\max}{}^{(B)}/\eta^{(B)}$, while $\eta^{(A)}\eta^{(B)} = 1$. The maximum frequency in the phase factor of Eq. (3.10) near the focus is therefore $(\mathbf{f}\dot{\omega}_{\max}/\eta) + \mathbf{r}_c$. However, the coordinates have been normalized by $\mathbf{f}/\eta$; therefore

$$\Delta \leq \frac{1}{2\left(\dot{\omega}_{\max} + \dfrac{\eta \mathbf{r}_c}{\mathbf{f}}\right)}. \tag{3.15}$$

Thus, when $\mathbf{z} \approx \mathbf{f}$, relations (3.12) and (3.15) combine to yield

$$\frac{L_{\max}}{N_{\max}} \leq \min\left\{\frac{\mathbf{R}}{10}, \frac{1}{2\left(\dot{\omega}_{\max} + \dfrac{\eta \mathbf{r}_c}{\mathbf{f}}\right)}\right\}. \tag{3.16}$$

4. Calculate the final distribution from Eq. (3.11). The final array length will be

$$\tilde{L}_{\max} = \frac{\mathbf{f}N_{\max}}{\eta L_{\max}}. \tag{3.17}$$

B. Spherical Lens and the Stationary-Phase Approximation

With increasing numerical aperture and/or focal length, the method described in Subsection 3.A becomes impractical in terms of computer time and memory requirements. In this regime, however, the stationary-phase approximation applies, and we can directly calculate the Fourier transform of $t(x, y)$ in Eq. (3.1a). Defining $X = x/f$, $Y = y/f$, $X_c = x_c/f$, and $Y_c = y_c/f$, we write

$$\lambda^{-2}T\left(\frac{\sigma_x}{\lambda}, \frac{\sigma_y}{\lambda}\right) = \mathbf{f}^2 \int\int_{-\infty}^{\infty} \tilde{\tau}_0(fX, fY) \times \exp[-i2\pi \mathbf{f} W(X, Y)]\mathrm{d}X\mathrm{d}Y, \tag{3.18a}$$

where

$$W(X, Y) = [1 + (X - X_c)^2 + (Y - Y_c)^2]^{1/2} + \sigma_x X + \sigma_y Y. \tag{3.18b}$$

$W(X, Y)$ has a stationary point at

$$X_0 = X_c - \frac{\sigma_x}{(1 - \sigma_x{}^2 - \sigma_y{}^2)^{1/2}}, \tag{3.19a}$$

$$Y_0 = Y_c - \frac{\sigma_y}{(1 - \sigma_x{}^2 - \sigma_y{}^2)^{1/2}}. \tag{3.19b}$$

The Taylor-series expansion of $W(X, Y)$ around the stationary point is

$$\begin{aligned} W(X, Y) = {} & \sigma_x X_c + \sigma_y Y_c + (1 - \sigma_x{}^2 - \sigma_y{}^2)^{1/2} \\ & \times [1 + \tfrac{1}{2}(1 - \sigma_x{}^2)(X - X_0)^2 \\ & - \sigma_x\sigma_y(X - X_0)(Y - Y_0) \\ & + \tfrac{1}{2}(1 - \sigma_y{}^2)(Y - Y_0)^2] + \ldots . \end{aligned} \tag{3.20}$$

Replacing $W(X, Y)$ in Eq. (3.18a) and completing the stationary-phase approximation yields

$$\lambda^{-2}T\left(\frac{\sigma_x}{\lambda}, \frac{\sigma_y}{\lambda}\right) = \tilde{\tilde{\tau}}_0(\sigma_x, \sigma_y) \times \exp\{-i2\pi \mathbf{f}[(1 - \sigma_x{}^2 - \sigma_y{}^2)^{1/2} + \sigma_x X_c + \sigma_y Y_c]\}, \tag{3.21a}$$

where

$$\tilde{\tilde{\tau}}_0(\sigma_x, \sigma_y) = \left(\frac{-i\mathbf{f}}{1 - \sigma_x{}^2 - \sigma_y{}^2}\right) \times \tilde{\tau}_0\left[x_c - \frac{f\sigma_x}{(1 - \sigma_x{}^2 - \sigma_y{}^2)^{1/2}}, y_c - \frac{f\sigma_y}{(1 - \sigma_x{}^2 - \sigma_y{}^2)^{1/2}}\right]. \tag{3.21b}$$

$\tilde{\tilde{\tau}}_0(\sigma_x, \sigma_y)$ is a shifted, inverted, and scaled version of $\tilde{\tau}_0(x, y)$. The main attributes of this transformation are as follows:

1. $\tilde{\tau}_0$ is centered at (x_c, y_c), whereas $\tilde{\tilde{\tau}}_0$ is centered at the origin.
2. The radius of the exit pupil is $f \tan[\arcsin(\mathrm{NA})]$, whereas $\tilde{\tilde{\tau}}_0(\sigma_x, \sigma_y)$ has a radius NA.
3. The total incident power is conserved; i.e., $|\tilde{\tau}_0(\lambda\mathbf{x}, \lambda\mathbf{y})|^2$ and $|\tilde{\tilde{\tau}}_0(\sigma_x, \sigma_y)|^2$ have the same integral in their domains.

The scaling of $\tilde{\tau}_0(x, y)$ in Eq. (3.21b) is equivalent to replacing the distribution at the exit pupil of an aplanatic lens with that at the entrance pupil. Thus, given the input distribution to such a lens, no further scaling is required. (The shift to the center and the inversion are still necessary, however.)

Equation (3.21a) is now substituted into Eq. (2.2) to yield

$$\tilde{t}_{\alpha\beta}(\lambda\mathbf{x}, \lambda\mathbf{y}, \lambda\mathbf{z}) = \mathcal{F}^{-1}\{\exp\{i2\pi[(\mathbf{z} - \mathbf{f})(1 - \sigma_x{}^2 - \sigma_y{}^2)^{1/2} - \mathbf{x}_c\sigma_x - \mathbf{y}_c\sigma_y]\}\Psi_{\alpha\beta}(\sigma_x, \sigma_y)\tilde{\tilde{\tau}}_0(\sigma_x, \sigma_y)\}. \tag{3.22}$$

Equation (3.22) provides a simple expression for vector diffraction in the neighborhood of the focal plane. This equation is identical to the one derived by Wolf[1] and is valid only when the stationary-phase approximation applies. Note that, in the absence of aberrations, $\tilde{t}(x, y, z) = \tilde{t}^*(2x_c - x, 2y_c - y, 2f - z)$. (* denotes a complex conjugate.) This symmetry with respect to the focal point is a consequence of the stationary-phase approximation and its absence in a physical system is a manifestation of the breakdown of the approximation.

The extent of $\tilde{\tilde{\tau}}_0(\sigma_x, \sigma_y)$ in the $\sigma_x\sigma_y$ plane is $\sigma_{\max} = \mathrm{NA}$, which means that the sample spacing that ensures proper sampling of the exponential phase factor in Eq. (3.22) is

$$\frac{\Delta}{\mathbf{f}} \leq \min\left\{\frac{\mathrm{NA}}{10}, \frac{1}{2}\left\{\mathbf{r}_c + \frac{|\mathbf{z} - \mathbf{f}|\mathrm{NA}}{[1 - (\mathrm{NA})^2]^{1/2}}\right\}^{-1}\right\}. \tag{3.23}$$

For proper resolution in the $\mathbf{xy}$ plane we require that

$$L_{\max} \geq 10\mathbf{f}\mathrm{NA}. \tag{3.24}$$

Of course, if the incident distribution has fine features or if better resolution is required, the values of $N_{\max}$ and $L_{\max}$ must be adjusted accordingly. The final length of the array will be

$$\tilde{L}_{\max} = \frac{\mathbf{f}N_{\max}}{L_{\max}}. \tag{3.25}$$

C. Astigmatic Lens

An astigmatic lens with focal lengths f_x and f_y, a numerical aperture NA (to be defined below), and center coordinates (x_c, y_c), is represented by the following amplitude distribution at the exit pupil:

$$t(x, y) = \begin{cases} \tau_0(x, y)\exp\left(-i\frac{2\pi}{\lambda}\left(\frac{2f_xf_y}{f_x+f_y}\right)\left\{1+\left(\frac{f_x+f_y}{2f_xf_y}\right)\left[\frac{(x-x_c)^2}{f_x}+\frac{(y-y_c)^2}{f_y}\right]\right\}^{1/2}\right) \\ 0 \qquad \left\{\frac{f_x+f_y}{2f_xf_y}\left[\frac{(x-x_c)^2}{f_x}+\frac{(y-y_c)^2}{f_y}\right]\right\}^{1/2} > \tan[\arcsin(\mathrm{NA})] \end{cases}. \quad (3.26)$$

This is not necessarily the simplest function to represent an astigmatic lens. Other functions may be suggested, and the following treatment would apply equally to them. The above function, however, has three appealing properties. The first is that when $f_x = f_y$ it reduces to the spherical lens of Eq. (3.1). The second is that in the paraxial approximation it becomes

$$t(x, y) = \tau_0(x, y)\exp\left\{-i\frac{\pi}{\lambda}\left[\frac{(x-x_c)^2}{f_x}+\frac{(y-y_c)^2}{f_y}\right]\right\}, \quad (3.27)$$

which clearly shows that f_x and f_y correspond to the curvature of the wave front along the x and y directions. The third property is that the exit pupil is an ellipse rather than a circle; this allows a single value of η to minimize the oscillations along both x and y axes. The optimum η is obtained from Appendix B with $\theta_1 = 0$ and $\theta_2 = \arcsin(\mathrm{NA})$. θ_2 is the half-angle subtended by the lens axis parallel to x at a distance of $[2f_x{}^2f_y/(f_x + f_y)]^{1/2}$. Equivalently, θ_2 is the half-angle subtended by the axis parallel to y at a distance of $[2f_xf_y{}^2/(f_x + f_y)]^{1/2}$.

The treatment of the astigmatic lens parallels that of the spherical lens in Subsection 3.A. The main steps are outlined below.

1. Calculate $\tau(x, y)$ from the following relation:

$$\tau(x, y) = \tau_0(x, y)\exp\left[-i2\pi\left(\frac{2\mathbf{f}_x\mathbf{f}_y}{\mathbf{f}_x+\mathbf{f}_y}\right)\times\left(\left\{1+\left(\frac{\mathbf{f}_x+\mathbf{f}_y}{2\mathbf{f}_x\mathbf{f}_y}\right)\left[\frac{(\mathbf{x}-\mathbf{x}_c)^2}{\mathbf{f}_x}+\frac{(\mathbf{y}-\mathbf{y}_c)^2}{\mathbf{f}_y}\right]\right\}^{1/2} - \frac{1}{2}\eta\left(\frac{\mathbf{f}_x+\mathbf{f}_y}{2\mathbf{f}_x\mathbf{f}_y}\right)\left[\frac{(\mathbf{x}-\mathbf{x}_c)^2}{\mathbf{f}_x}+\frac{(\mathbf{y}-\mathbf{y}_c)^2}{\mathbf{f}_y}\right]\right)\right]. \quad (3.28)$$

The sample spacings Δ_x and Δ_y must satisfy

$$\Delta_x \le \min\left\{\frac{\mathbf{R}_x}{10}, \frac{\left(\frac{1}{2}+\frac{f_x}{2f_y}\right)^{1/2}}{2\dot{\omega}_{\max}}\right\}, \quad (3.29a)$$

$$\Delta_y \le \min\left\{\frac{\mathbf{R}_y}{10}, \frac{\left(\frac{1}{2}+\frac{f_y}{2f_x}\right)^{1/2}}{2\dot{\omega}_{\max}}\right\}. \quad (3.29b)$$

Here R_x and R_y are the half-axes of the (elliptical) exit pupil, and $\dot{\omega}_{\max}$, a function of NA, is given in Fig. 18 of Appendix B.

2. Calculate $h(u, v)$ as follows:

$$h(u, v) = -i\frac{(\mathbf{f}_x\mathbf{f}_y)^{1/2}}{\eta}\exp\left\{i\pi\eta\left[\frac{(u+\mathbf{x}_c)^2}{\mathbf{f}_x}+\frac{(v+\mathbf{y}_c)^2}{\mathbf{f}_y}\right]\right\} \times \mathcal{F}\left\{\tau\left(\frac{\lambda\mathbf{f}_x}{\eta}X, \frac{\lambda\mathbf{f}_y}{\eta}Y\right)\right\}. \quad (3.30)$$

Note that the x and y axes are normalized differently in Eq. (3.30). The limits imposed on $L_{\max}$ and L_{may} can be obtained by considerations similar to those that led to relation (3.14). Thus we have

$$L_{\max} \ge \max\left\{10\mathbf{R}_x, \frac{2\mathbf{f}_x}{\eta}\left[\frac{\dot{\omega}_{\max}}{\left(\frac{1}{2}+\frac{f_x}{2f_y}\right)^{1/2}}+\frac{1}{2\mathbf{R}_x}\right]+2|\mathbf{x}_c|\right\}. \quad (3.31)$$

A similar relation is obtained for L_{may}.

3. Compute $g(\sigma_x, \sigma_y)$ as follows:

$$g(\sigma_x, \sigma_y) = \exp\left\{i2\pi\mathbf{z}\left[(1-\sigma_x{}^2-\sigma_y{}^2)^{1/2}+\frac{\mathbf{f}_x}{2\eta\mathbf{z}}\sigma_x{}^2+\frac{\mathbf{f}_y}{2\eta\mathbf{z}}\sigma_y{}^2\right]\right\} \times \exp[-i2\pi(\mathbf{x}_c\sigma_x+\mathbf{y}_c\sigma_y)]\mathcal{F}\{h(u, v)\}. \quad (3.32)$$

If $\mathbf{f}_x$ and $\mathbf{f}_y$ are not too far apart, then in the neighborhood of the focus one can use the same approximations that led to relation (3.16) and conclude that in addition to relation (3.31) the following inequality must be satisfied:

$$\frac{L_{\max}}{N_{\max}} \le \min\left\{\frac{\mathbf{R}_x}{10}, \frac{\left(\frac{1}{2}+\frac{f_x}{2f_y}\right)^{1/2}}{2\left(\dot{\omega}_{\max}+\frac{\eta|\mathbf{x}_c|}{\mathbf{f}_x}\right)}\right\}. \quad (3.33)$$

A similar relationship exists for $L_{\mathrm{may}}/N_{\mathrm{may}}$.

4. Calculate the final distribution from

$$\tilde{t}_{\alpha\beta}(\lambda\mathbf{x}, \lambda\mathbf{y}, \lambda\mathbf{z}) = \mathcal{F}^{-1}\{\Psi_{\alpha\beta}(\sigma_x, \sigma_y)g(\sigma_x, \sigma_y)\}. \quad (3.34)$$

The final array dimensions will be

$$\tilde{L}_{\max} = \frac{\mathbf{f}_xN_{\max}}{\eta L_{\max}}, \quad (3.35a)$$

$$\tilde{L}_{\mathrm{may}} = \frac{\mathbf{f}_yN_{\mathrm{may}}}{\eta L_{\mathrm{may}}}. \quad (3.35b)$$

D. Astigmatic Lens and the Stationary-Phase Approximation

When the focal lengths are sufficiently large, the distribution of relation (3.26) can be Fourier transformed directly, provided that one invokes the stationary-phase approximation. Under these conditions,

$$\lambda^{-2}T\left(\frac{\sigma_x}{\lambda}, \frac{\sigma_y}{\lambda}\right) = \tilde{\tau}_0(\sigma_x, \sigma_y)\exp\left(-i2\pi\left\{\left(\frac{2\mathbf{f}_x\mathbf{f}_y}{\mathbf{f}_x + \mathbf{f}_y}\right)\right.\right.$$
$$\left.\left.\times\left[1 - \left(\frac{1}{2} + \frac{\mathbf{f}_x}{2\mathbf{f}_y}\right)\sigma_x^2 - \left(\frac{1}{2} + \frac{\mathbf{f}_y}{2\mathbf{f}_x}\right)\sigma_y^2\right]^{1/2} + \mathbf{x}_c\sigma_x + \mathbf{y}_c\sigma_y\right\}\right), \tag{3.36a}$$

where

$$\tilde{\tau}_0(\sigma_x, \sigma_y) = \frac{-i(\mathbf{f}_x\mathbf{f}_y)^{1/2}}{1 - \left(\frac{1}{2} + \frac{\mathbf{f}_x}{2\mathbf{f}_y}\right)\sigma_x^2 - \left(\frac{1}{2} + \frac{\mathbf{f}_y}{2\mathbf{f}_x}\right)\sigma_y^2}$$
$$\times \tau_0\left\{x_c - \frac{f_x\sigma_x}{\left[1 - \left(\frac{1}{2} + \frac{\mathbf{f}_x}{2\mathbf{f}_y}\right)\sigma_x^2 - \left(\frac{1}{2} + \frac{\mathbf{f}_y}{2\mathbf{f}_x}\right)\sigma_y^2\right]^{1/2}}, y_c - \frac{f_y\sigma_y}{\left[1 - \left(\frac{1}{2} + \frac{\mathbf{f}_x}{2\mathbf{f}_y}\right)\sigma_x^2 - \left(\frac{1}{2} + \frac{\mathbf{f}_y}{2\mathbf{f}_x}\right)\sigma_y^2\right]^{1/2}}\right\}. \tag{3.36b}$$

Substituting Eq. (3.36a) into Eq. (2.2) yields

$$\tilde{t}_{\alpha\beta}(\lambda\mathbf{x}, \lambda\mathbf{y}, \lambda\mathbf{z}) = \mathcal{F}^{-1}\left\{\exp\left(i2\pi\left\{\mathbf{z}(1 - \sigma_x^2 - \sigma_y^2)^{1/2} - \left(\frac{2\mathbf{f}_x\mathbf{f}_y}{\mathbf{f}_x + \mathbf{f}_y}\right)\right.\right.\right.$$
$$\times\left[1 - \left(\frac{1}{2} + \frac{\mathbf{f}_x}{2\mathbf{f}_y}\right)\sigma_x^2 - \left(\frac{1}{2} + \frac{\mathbf{f}_y}{2\mathbf{f}_x}\right)\sigma_y^2\right]^{1/2}$$
$$\left.\left.\left. - \mathbf{x}_c\sigma_x - \mathbf{y}_c\sigma_y\right\}\right)\Psi_{\alpha\beta}(\sigma_x, \sigma_y)\tilde{\tau}_0(\sigma_x, \sigma_y)\right\}. \tag{3.37}$$

The proper sample spacing in the x direction is

$$\frac{\Delta_x}{\mathbf{f}_x} \le \min\left\{\frac{\mathrm{NA}}{10\left(\frac{1}{2} + \frac{\mathbf{f}_x}{2\mathbf{f}_y}\right)^{1/2}}, \frac{1}{2}\left(|\mathbf{x}_c| + \left|\frac{\mathbf{f}_x\mathrm{NA}}{\left\{\left(\frac{1}{2} + \frac{\mathbf{f}_x}{2\mathbf{f}_y}\right)[1 - (\mathrm{NA})^2]\right\}^{1/2}} - \frac{\mathbf{z}\mathrm{NA}}{\left[\frac{1}{2} + \frac{\mathbf{f}_x}{2\mathbf{f}_y} - (\mathrm{NA})^2\right]^{1/2}}\right|\right)^{-1}\right\}. \tag{3.38}$$

A similar expression exists for Δ_y. The length of the array is restricted as follows:

$$L_{\max} \ge \frac{10\mathbf{f}_x\mathrm{NA}}{\left(\frac{1}{2} + \frac{\mathbf{f}_x}{2\mathbf{f}_y}\right)^{1/2}}, \tag{3.39}$$

with a similar relationship for L_{may}. The final array dimensions are

$$\tilde{L}_{\max} = \frac{\mathbf{f}_x N_{\max}}{L_{\max}}, \tag{3.40a}$$

$$\tilde{L}_{\mathrm{may}} = \frac{\mathbf{f}_y N_{\mathrm{may}}}{L_{\mathrm{may}}}. \tag{3.40b}$$

E. Ring Lens

The ring lens is a circularly symmetric lens with a cross section as shown in Fig. 2. A potential application of the ring lens is focus-error detection in optical disk systems.[12] A collimated beam is brought to focus by this lens on a ring of radius R_0 at the focal plane. The central region of the lens ($r < R_1$) is flat, and it is assumed that the light in this region is unaffected by the lens. The aperture radius is R_2. For lens-center coordinates (x_c, y_c), the exit pupil distribution is written as

$$t(x, y) = \tau_0(x, y)\exp\left[-i\frac{2\pi}{\lambda}(f^2 + \{[(x - x_c)^2 + (y - y_c)^2]^{1/2} - R_0\}^2)^{1/2}\right]. \tag{3.41}$$

Again, as in the case of a spherical lens, a quadratic term is factored out and treated analytically. The necessary steps are summarized below.

1. Calculate $\tau(x, y)$ with optimum η (see Appendix C) from the relation

$$\tau(x, y) = \begin{cases} \tau_0(x, y)\exp\left\{-\frac{i2\pi f}{\lambda}\left[\left(1 + \left\{\left[\frac{(x - x_c)^2 + (y - y_c)^2}{f^2}\right]^{1/2} - \frac{R_0}{f}\right\}^2\right)^{1/2} - \frac{1}{2}\eta\frac{(x - x_c)^2 + (y - y_c)^2}{f^2}\right]\right\} & \\ 1 \quad [(x - x_c)^2 + (y - y_c)^2]^{1/2} \le R_1 & \\ 0 \quad [(x - x_c)^2 + (y - y_c)^2]^{1/2} \ge R_2 & \end{cases}. \tag{3.42}$$

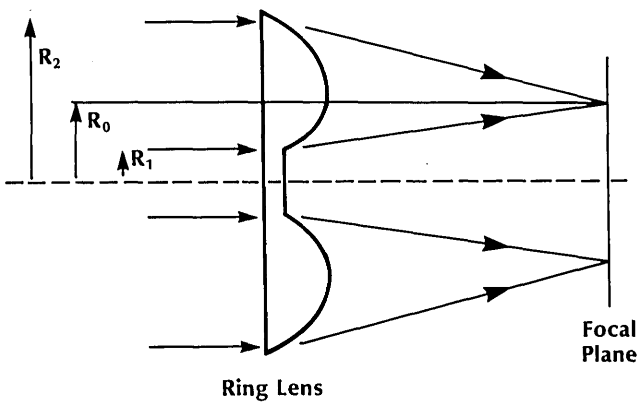

Fig. 2. Cross section of a ring lens. The central region ($r < R_1$) is flat and does not affect the incident beam. The curved surface peaks at $r = R_0$, and the aperture radius of the lens is R_2. A collimated beam is brought to focus by this lens on a sharp ring of radius R_0 at the focal plane. The amplitude distribution at the exit pupil is given by Eq. (3.41), and, in the absence of aberrations, the ring width is diffraction limited.

The spacing between the samples in the **xy** plane must satisfy relation (3.16).

2. Determine $h(u, v)$ from Eq. (3.8). The restriction on L_{max} is given by relation (3.14).

3. Calculate $g(\sigma_x, \sigma_y)$ from Eq. (3.10) and the final distribution from Eq. (3.11).

4. RESULTS AND DISCUSSION

Example 1

We study the diffraction pattern from a circular aperture of radius **R** = 500, illuminated with a plane uniform wave (**C** = 0). The integrated intensity within the aperture is set to unity. We choose $N_{max} = N_{may} = 256$, since it is a convenient array dimension for performing FFT's, and let $L_{max} = L_{may} = 5000$. (On a VAX 11/780 computer each 256 × 256 FFT takes only ~10 sec.) Now, for distances **z** that are not too far from the aperture, both direct and extended Fresnel techniques can be applied. A good guide for selecting distances in this

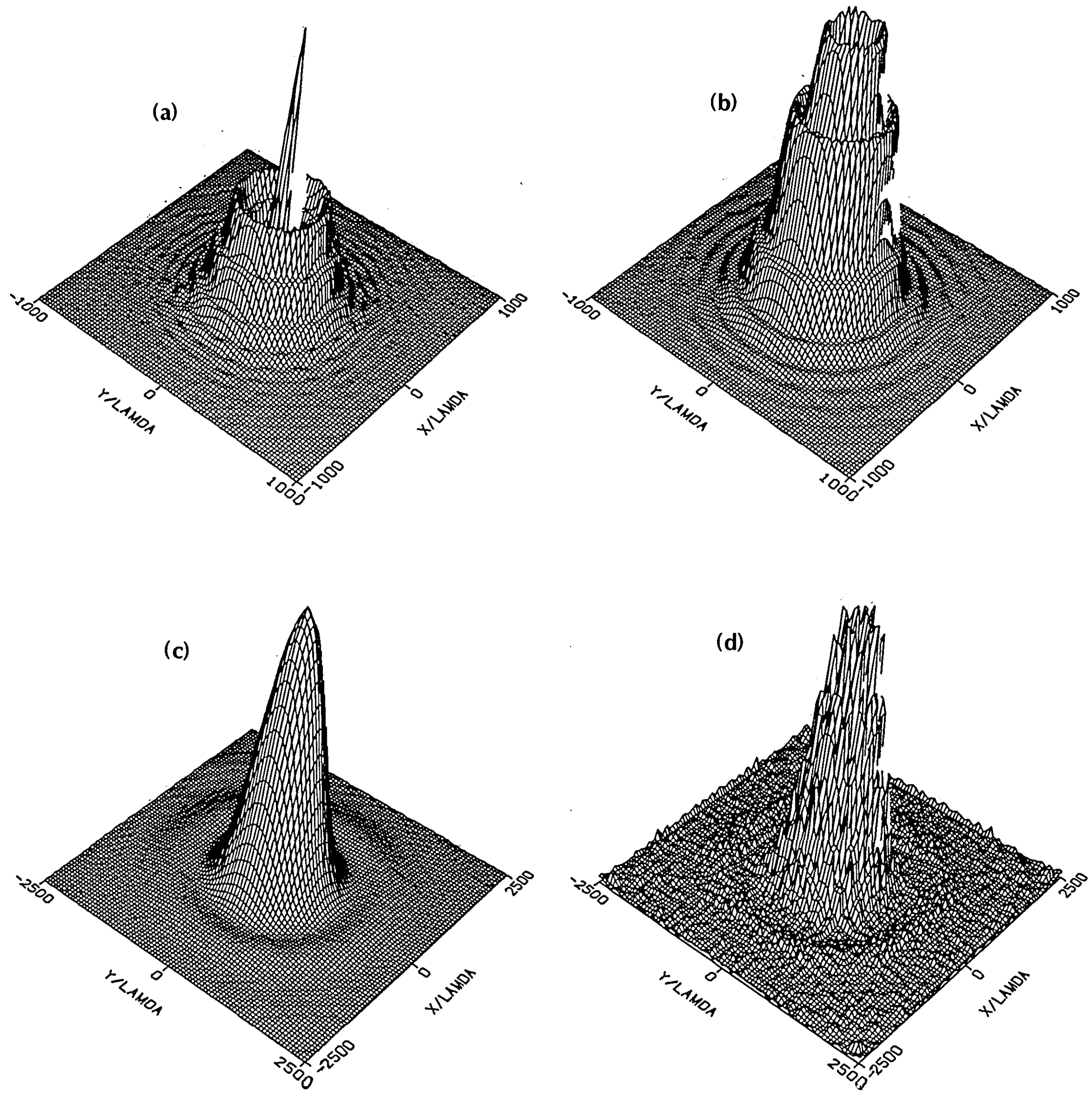

Fig. 3. Circular aperture of radius $R = 500\lambda$ illuminated with a plane uniform wave. (a) Intensity pattern at a distance of 83,333λ from the aperture; both direct and extended Fresnel techniques give the same result. (b) Intensity distribution at $z = 125{,}000\lambda$. Again both methods give the same result. (c) Intensity pattern at $z = 1{,}000{,}000\lambda$ obtained by the extended Fresnel method. (d) Same as (c) but with the direct Fresnel method. In all cases $N_{max} = N_{may} = 256$ and $L_{max} = L_{may} = 5000$.

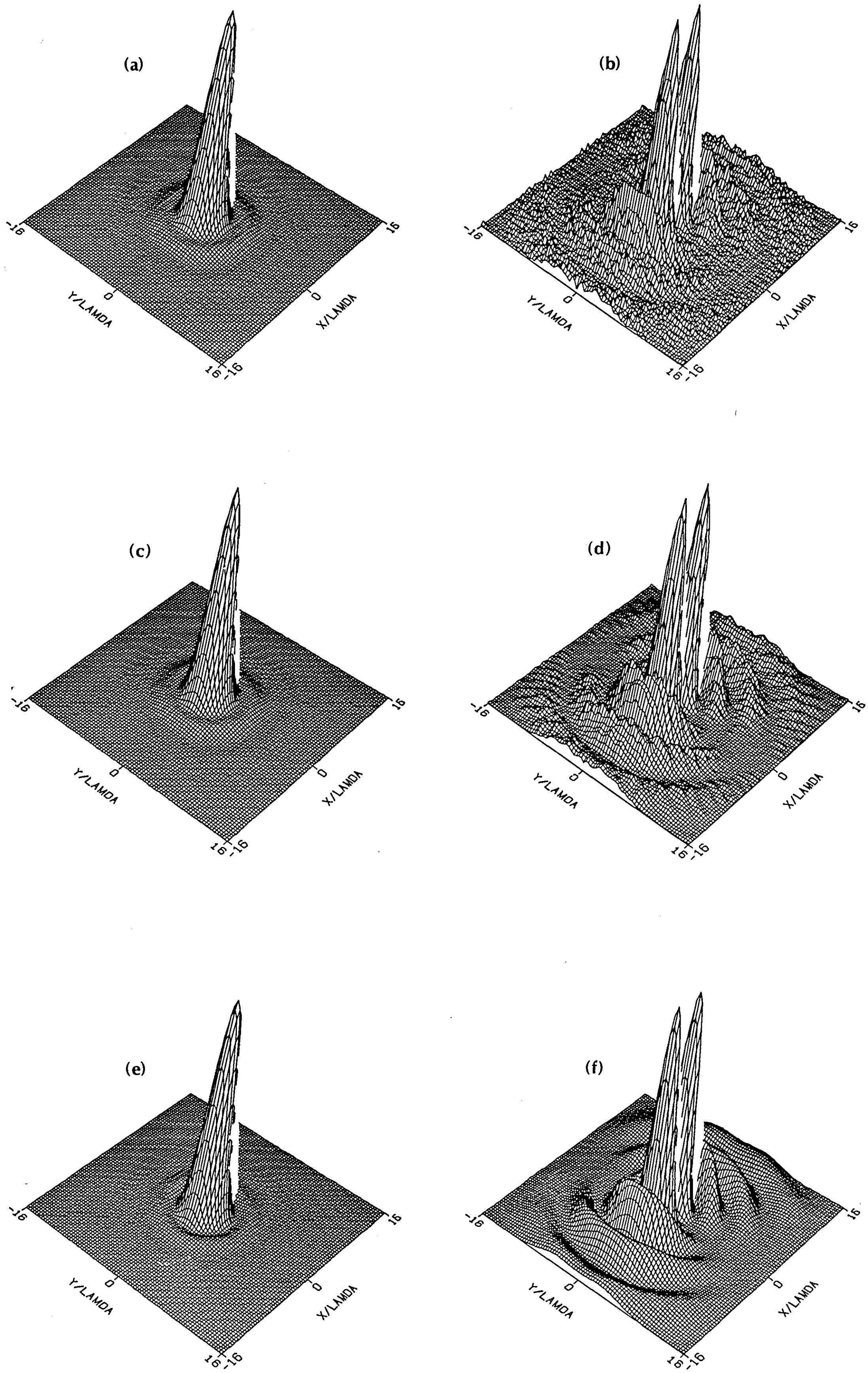

Fig. 4. Circular aperture of radius $R = 3\lambda$ illuminated with a plane uniform wave, polarized in the x direction. The intensity patterns are calculated at a distance of 20λ from the aperture. (a) and (b) show, respectively, the x and the z components of polarization obtained by the direct Fresnel method. (c) and (d) show the results of extended Fresnel calculations, and (e) and (f) show the results obtained from the Fraunhofer diffraction formula.

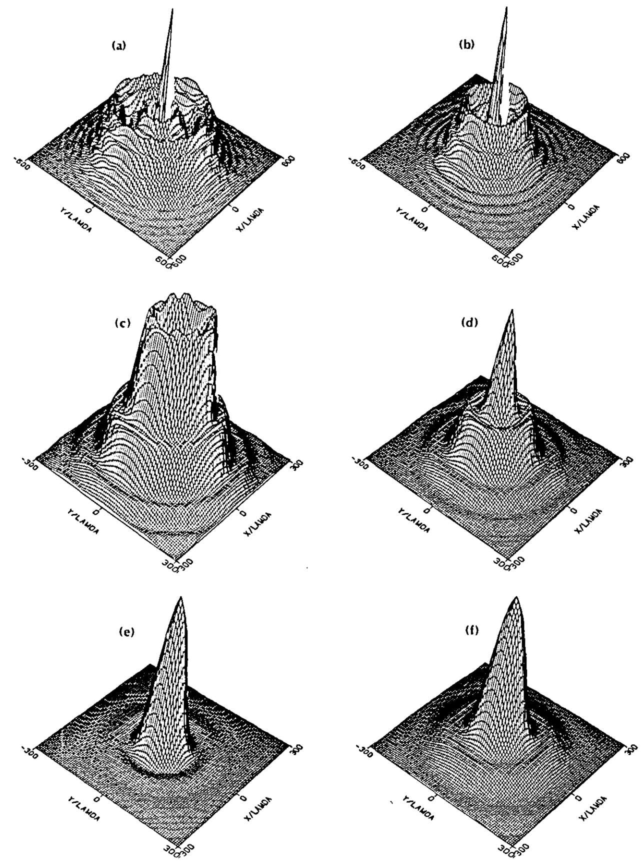

Fig. 5. Circular aperture of radius $R = 1000\lambda$ illuminated with a uniform wave of curvature $\mathbf{C} = 5 \times 10^{-6}$ corresponding to a positive spherical lens of $\mathbf{f} = 200{,}000\lambda$ and NA = 0.005. The intensity patterns are calculated with the extended Fresnel technique, using $N_{\max} = N_{\text{may}} = 512$ and $L_{\max} = L_{\text{may}} = 10{,}000$. (a) $\mathbf{z} = 100{,}000$, (b) $\mathbf{z} = 125{,}000$, (c) $\mathbf{z} = 150{,}000$, (d) $\mathbf{z} = 160{,}000$, (e) $\mathbf{z} = 200{,}000$, and (f) $\mathbf{z} = 240{,}000$.

not-too-far regime is the Fresnel number N defined by the relation[13]

$$\mathbf{z} = \frac{1}{N}\mathbf{R}^2 - \frac{N}{4}. \tag{4.1}$$

For instance, $N = 3$ corresponds to $\mathbf{z} = 83{,}333$. The two methods give identical results in this case, and the resulting intensity pattern is shown in Fig. 3(a). A similar situation occurs when $N = 2$ and $\mathbf{z} = 125{,}000$. Both direct and extended Fresnel methods give the same result, which is shown in Fig. 3(b).

As $\mathbf{z}$ increases, however, the advantages of the extended method become apparent. Figure 3(c) shows the intensity pattern at $\mathbf{z} = 1{,}000{,}000$, calculated with the extended method, whereas Fig. 3(d) shows the result of direct computation. It is obvious that, for the direct method to work at large distances, the array size must increase, but the extended method can perform reliably even at distances that are deep in the far-field region. To check the validity of the extended method, we calculated the Fraunhofer pattern at $\mathbf{z} = 1{,}000{,}000$; the resulting pattern was identical to that shown in Fig. 3(c).

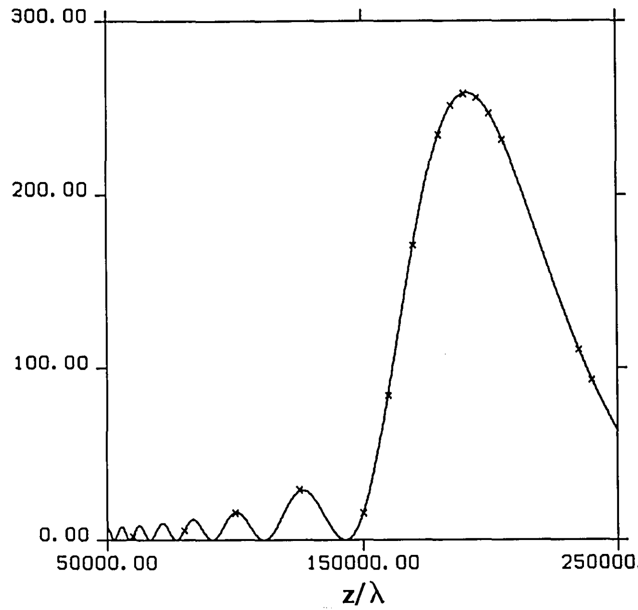

Fig. 6. Circular aperture of radius $R = 1000\lambda$ illuminated with a uniform wave of curvature $\mathbf{C} = -5 \times 10^{-6}$. Intensity on the optical axis is shown here as a function of distance from the aperture. The solid curve is calculated from the analytic expression derived in Ref. 9. The crosses are obtained by numerical computations using direct (or extended) Fresnel method.

Example 2

Consider a circular aperture of radius $\mathbf{R} = 3$, illuminated with a plane uniform beam polarized along $\mathbf{x}$. The integrated intensity within the aperture is unity. Let $N_{\max} = N_{\text{may}} = 256$ and $L_{\max} = L_{\text{may}} = 30$. Figure 4 shows the intensity patterns

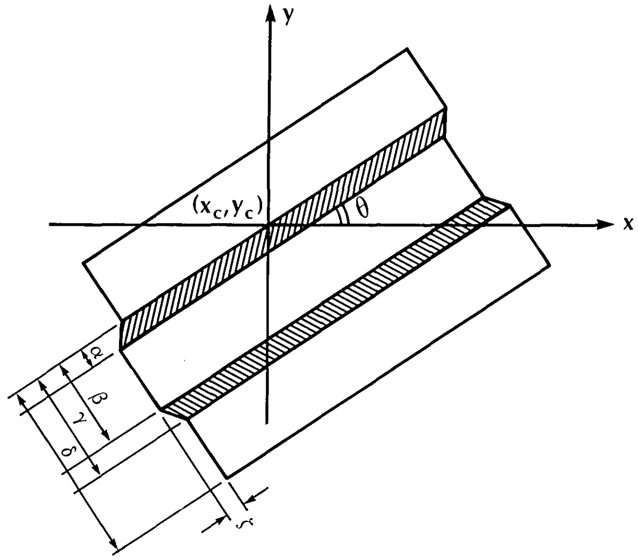

Fig. 7. Geometry of groove structure for a transmission phase diffraction grating. All parameters are in units of the wavelength λ.

for the x and z components of polarization at a distance of $\mathbf{z} = 20$ from the aperture. (The y component was smaller than the numerical errors and could not be computed.) For comparison the results obtained with direct Fresnel, extended Fresnel, and Fraunhofer techniques are all shown in this figure.

Example 3

A circular aperture of radius $\mathbf{R} = 1000$ is illuminated with a uniform wave front of curvature $\mathbf{C} = -5 \times 10^{-6}$. (The situation is similar to that of an incident plane wave on a positive spherical lens of $\mathbf{f} = 200{,}000$ and NA = 0.005.) The intensity distributions at various distances from the aperture are shown in Fig. 5. Note the asymmetry with respect to the focal plane by comparing Fig. 5(d) with Fig. 5(f). This asymmetry is well known for lenses of small numerical aperture, and, in fact, an analytic expression for the axial intensity of such systems was derived by Mahajan.[9] We have reproduced Mahajan's results in Fig. 6 (solid curve) and shown several instances of our own direct (or extended) Fresnel computations (crosses). The agreement is extreme-

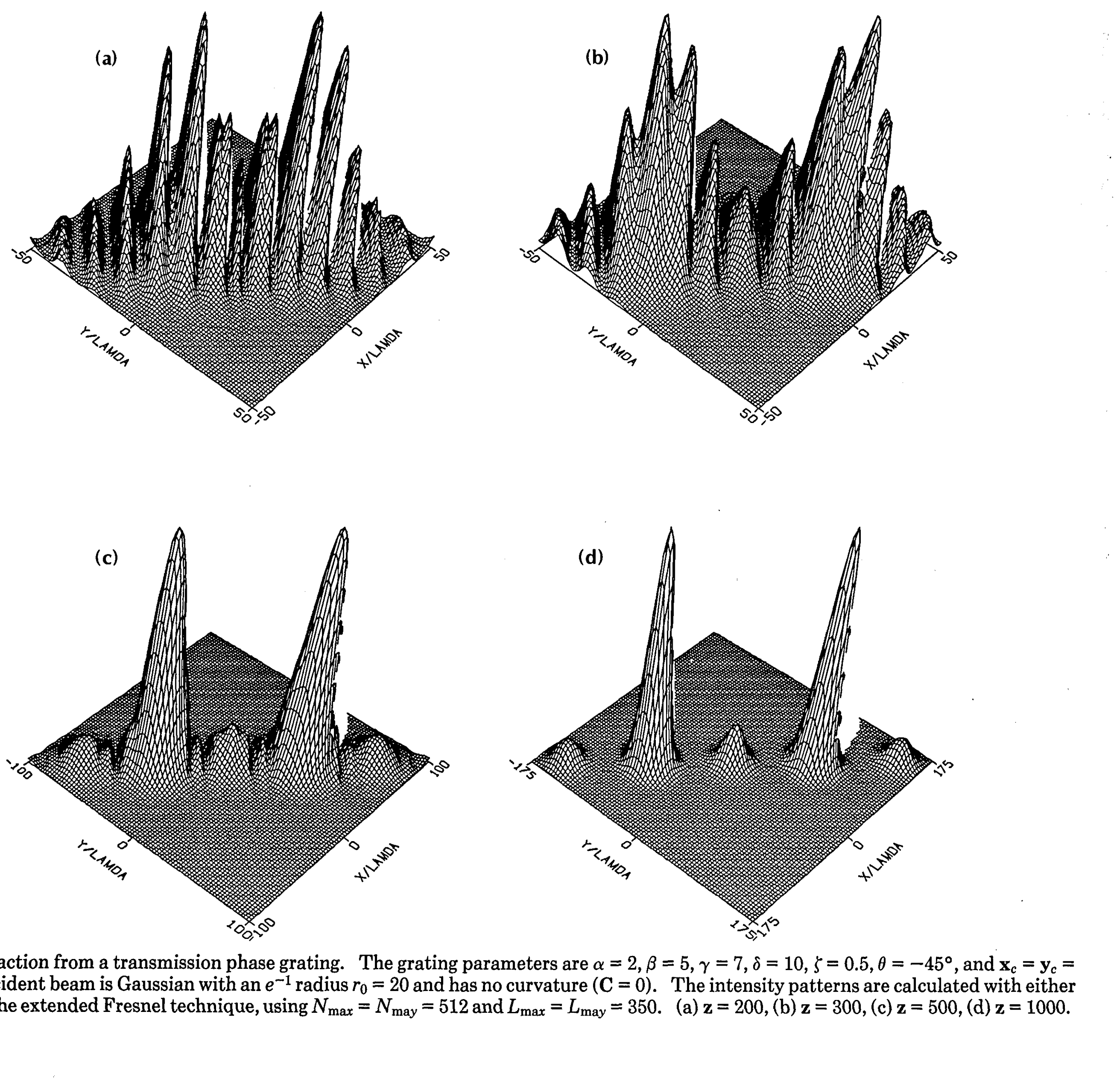

Fig. 8. Diffraction from a transmission phase grating. The grating parameters are $\alpha = 2$, $\beta = 5$, $\gamma = 7$, $\delta = 10$, $\zeta = 0.5$, $\theta = -45°$, and $\mathbf{x}_c = \mathbf{y}_c = 1.06$. The incident beam is Gaussian with an e^{-1} radius $r_0 = 20$ and has no curvature ($\mathbf{C} = 0$). The intensity patterns are calculated with either the direct or the extended Fresnel technique, using $N_{max} = N_{may} = 512$ and $L_{max} = L_{may} = 350$. (a) $\mathbf{z} = 200$, (b) $\mathbf{z} = 300$, (c) $\mathbf{z} = 500$, (d) $\mathbf{z} = 1000$.

ly good and shows the power and accuracy of the numerical method.

Example 4
With reference to Fig. 7, a transmission phase diffraction grating is specified with the parameters $\alpha, \beta, \gamma, \delta$, and ζ. The groove width is $\beta - \alpha$, and the land width is $\delta - \gamma$. The regions between land and groove have constant slope as determined by α and $\gamma - \beta$. If sharp boundaries are desired, one should set $\alpha = 0$ and $\beta = \gamma$. For further flexibility we have allowed the grating center (x_c, y_c) and orientation angle θ to be parameters as well. The aperture radius is R. If we assume that 10 samples per period of the grating are sufficient (this may not always be a good assumption) and that the incident beam is uniform with curvature $\mathbf{C}$, the restriction on sample spacing will be

$$\Delta < \left[\frac{10}{\delta} + \frac{2|\mathbf{C}|\mathbf{R}}{(1+\mathbf{C}^2\mathbf{R}^2)^{1/2}}\right]^{-1}. \tag{4.2}$$

The maximum spatial frequency is

$$\sigma_{\max} = \frac{|\mathbf{C}|\mathbf{R}}{(1+\mathbf{C}^2\mathbf{R}^2)^{1/2}} + \frac{1}{\delta}, \tag{4.3}$$

which is used in relation (2.5) to determine $L_{\max}$ for direct Fresnel calculations. For Fraunhofer calculations $L_{\max} = 10\mathbf{R}$ should be sufficient, and for extended Fresnel computations relation (2.11) applies. In the latter case, Δ must also satisfy relation (2.12).

Figure 8 shows the intensity patterns at various distances from a grating with parameters $\alpha = 2, \beta = 5, \gamma = 7, \delta = 10, \zeta = 0.5, \theta = -45°$, and $\mathbf{x}_c = \mathbf{y}_c = 1.06$. The incident beam is Gaussian with an e^{-1} radius $r_0 = 20$ and no curvature ($\mathbf{C} = 0$). Both direct and extended Fresnel methods give the near-field results in Figs. 8(a)–8(c), but the distribution in Fig. 8(d) must be calculated with the extended technique.

Example 5
Consider a cylindrical lens of focal length f and aperture radius R. The cylinder axis has an angle θ with the x axis, and the lens-center coordinates are (x_c, y_c). The aperture function is thus

$$\begin{aligned} t(x, y) &= \tau_0(x, y)\exp\left(-i\frac{2\pi}{\lambda}\{f^2 + [(x - x_c)\sin\theta - (y - y_c)\cos\theta]^2\}^{1/2}\right) \\ &= 0 \qquad [(x - x_c)^2 + (y - y_c)^2] > R^2. \end{aligned} \tag{4.4}$$

If we assume that the incident beam has a curvature $\mathbf{C}$, the spacing between samples must satisfy

$$\Delta \le \min\left\{\frac{\mathbf{R}}{10}, \left[2\mathrm{NA} + \frac{2|\mathbf{C}|\mathbf{R}}{(1+\mathbf{C}^2\mathbf{R}^2)^{1/2}}\right]^{-1}\right\}. \tag{4.5}$$

The maximum spatial frequency is

$$\sigma_{\max} = \mathrm{NA} + \frac{|\mathbf{C}|\mathbf{R}}{(1+\mathbf{C}^2\mathbf{R}^2)^{1/2}} + \frac{1}{2\mathbf{R}}, \tag{4.6}$$

which is used in relation (2.5) to determine $L_{\max}$ for direct Fresnel calculations. For Fraunhofer calculations $L_{\max} = 10\mathbf{R}$ should be sufficient, and for extended Fresnel computations relation (2.11) applies. In the latter case Δ must also satisfy relation (2.12).

Figure 9 shows the intensity pattern in the neighborhood of the focus for a cylindrical lens with $\mathbf{R} = 2500$, $\mathbf{f} = 10^6$, $\theta = 45°$, and $\mathbf{x}_c = \mathbf{y}_c = 0$. The incident beam is a plane wave with a curvature $\mathbf{C} = 0$. For these computations $N_{\max} = 512$ and $L_{\max} = 40{,}000$.

Example 6
Consider a spherical lens with a NA = 0.5 and a focal length $f = 3500\lambda$. Let the incident beam be plane, linearly polarized along the x axis, and with a total power of unity at the entrance pupil. Also assume that the lens is aberration free and satisfies Abbe's sine condition. Figure 10 shows the intensity patterns for the three components of polarization at the focal plane. The x component has 93% of the incident power and is similar to the classical Airy pattern. The y component has less than 0.1% of the power but shows the four peaks expected from geometrical considerations. The remaining 7% of the power is in the z component shown in Fig. 10(c). This time we observe two peaks, separated along the direction of incident polarization (x), also as expected from geometrical optics. Figure 11 shows the intensity patterns for the x component at 5λ and 10λ away from the focal plane. All the results are obtained by the exact method, using $L_{\max} = 20{,}000$ and $N_{\max} = 980$.

Since the stationary-phase approximation also applies here, the results are in good agreement with the classical ones.[2] The particular set of parameters in this example were chosen, however, to show the practicality of the exact method for relatively large numerical apertures; the focal length and the numerical aperture are typical of the microlenses now being used in optical disk systems.

Example 7
We analyze the case of an astigmatic lens with $\mathbf{f}_x = 20{,}000$, $\mathbf{f}_y = 20{,}200$, and NA = 0.15. The incident beam is plane and uniform, and the effects of polarization are ignored. Figure 12 shows plots of intensity at the two focal planes and at a plane halfway between them. Both the exact method and the stationary-phase approximation yield the same results.

Example 8
Consider a ring lens with $\mathbf{R}_1 = 50$, $\mathbf{R}_0 = 100$, $\mathbf{R}_2 = 2500$, and a focal length $\mathbf{f} = 25{,}000$. The incident beam is plane and uniform, and the polarization effects are ignored. Figure 13 shows the intensity patterns at and near the focal plane, calculated with $N_{\max} = N_{\mathrm{may}} = 512$ and $L_{\max} = L_{\mathrm{may}} = 25{,}000$.

APPENDIX A

Consider the function

$$\omega_\eta(r) = (1 - r^2)^{1/2} + \tfrac{1}{2}\eta r^2, \qquad r_1 \le r \le r_2, \tag{A1}$$

where $0 \le r_1 \le r_2 \le 1$ and η is a real parameter. The objective is to find the value of η that minimizes the maximum of $|\dot{\omega}_\eta(r)|$ in the interval $[r_1, r_2]$. $\dot{\omega}_\eta(r)$ is the derivative of $\omega_\eta(r)$ with respect to r and is given by

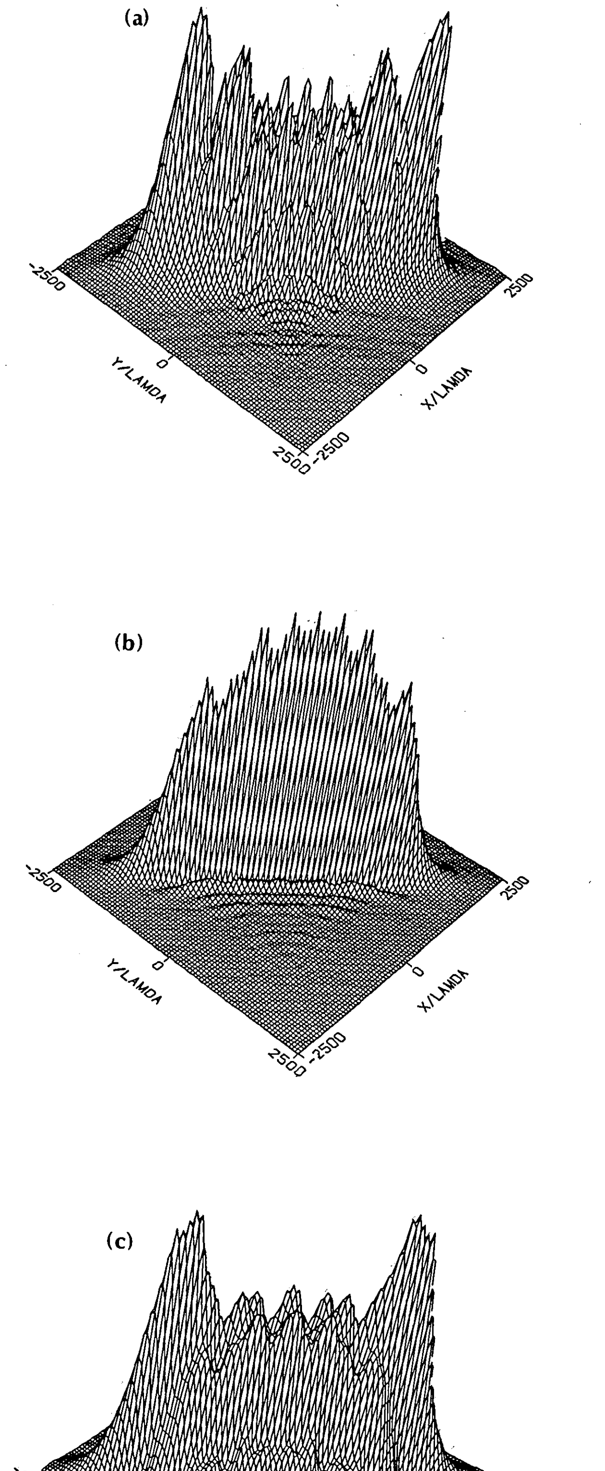

Fig. 9. Cylindrical lens with a focal length $f = 10^6\lambda$ and the aperture radius $R = 2500\lambda$. The incident beam is plane and uniform. The intensity patterns are obtained with the direct Fresnel method, using $N_{max} = N_{may} = 512$ and $L_{max} = L_{may} = 40{,}000$. (a) $\mathbf{z} = 0.75 \times 10^6$; (b) $\mathbf{z} = 10^6$; (c) $\mathbf{z} = 1.25 \times 10^6$.

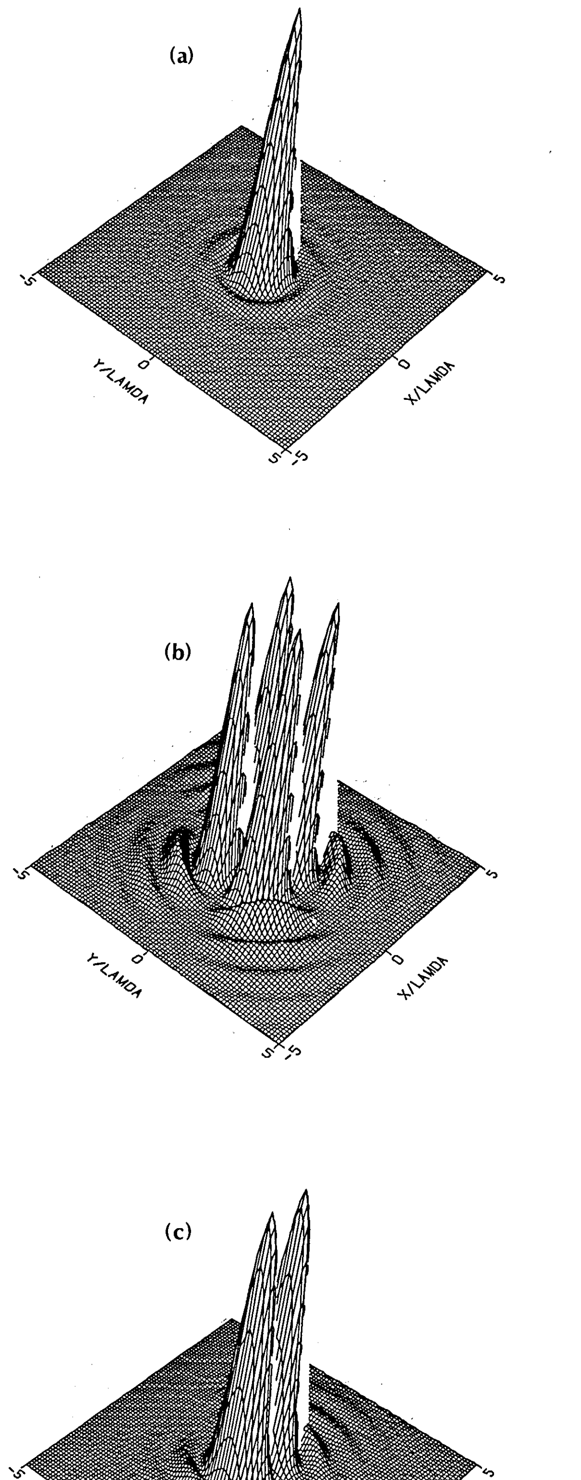

Fig. 10. Spherical lens with a numerical aperture NA = 0.5 and a focal length $f = 3500\lambda$, illuminated with a plane uniform wave, linearly polarized along the x axis. (a) Intensity pattern for the x component at the focus; (b) intensity pattern for the y component; (c) intensity distribution for the z component. For these computations, $N_{max} = N_{may} = 980$ and $L_{max} = L_{may} = 20{,}000$.

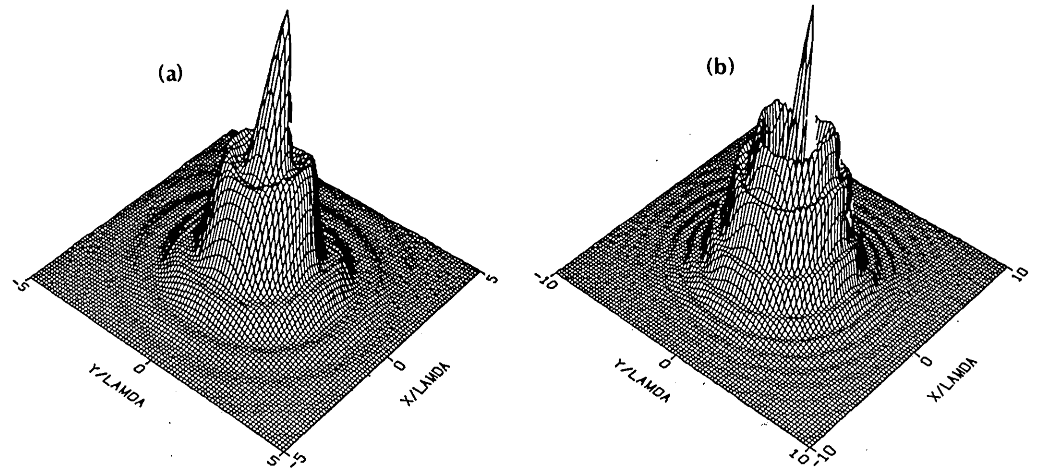

Fig. 11. Spherical lens with a numerical aperture NA = 0.5 and a focal length $f = 3500\lambda$, illuminated with a plane uniform wave, linearly polarized along the x axis. (a) Intensity pattern for the x component at a distance of 5λ from the focal plane; (b) intensity pattern for the x component at a distance of 10λ from the focal plane.

$$\dot{\omega}_\eta(r) = -(r^{-2} - 1)^{-1/2} + \eta r, \qquad r_1 \le r \le r_2. \tag{A2}$$

The function $\dot{\omega}_\eta(r)$ itself has the following derivative:

$$\ddot{\omega}_\eta(r) = -(1 - r^2)^{-3/2} + \eta, \qquad r_1 \le r \le r_2, \tag{A3}$$

which vanishes at

$$r_0 = (1 - \eta^{-2/3})^{1/2}. \tag{A4}$$

r_0 falls between r_1 and r_2, provided that

$$(1 - r_1{}^2)^{-3/2} \le \eta \le (1 - r_2{}^2)^{-3/2}. \tag{A5}$$

The value of $\dot{\omega}_\eta(r)$ at r_0 is

$$\dot{\omega}_\eta(r_0) = (\eta^{2/3} - 1)^{3/2}. \tag{A6}$$

Let us define θ_1 and θ_2 as follows:

$$\sin\theta_1 = r_1,$$
$$\sin\theta_2 = r_2; \tag{A7}$$

then the values of $\dot{\omega}_\eta(r)$ at r_1 and r_2 are

$$\dot{\omega}_\eta(r_1) = \eta \sin\theta_1 - \tan\theta_1, \tag{A8}$$

$$\dot{\omega}_\eta(r_2) = \eta \sin\theta_2 - \tan\theta_2. \tag{A9}$$

The maximum of $|\dot{\omega}_\eta(r)|$ over $[r_1, r_2]$, which will be referred to as $\dot{\omega}_{\max}$, is at r_1 or r_2 or, in case r_0 happens to be within the interval, at r_0. Thus, among Eqs. (A6), (A8), and (A9), one has the maximum absolute value. Figure 14 shows a plot of these three functions versus η. Note that, according to relation (A5), the range of η over which r_0 falls between r_1 and r_2 is

$$\frac{1}{\cos^3\theta_1} \le \eta \le \frac{1}{\cos^3\theta_2}. \tag{A10}$$

The value of η at which $\dot{\omega}_\eta(r_1) = -\dot{\omega}_\eta(r_2)$ is

$$\eta_0 = \frac{\tan\theta_1 + \tan\theta_2}{\sin\theta_1 + \sin\theta_2}. \tag{A11}$$

If $1/\cos^3\theta_1 \ge \eta_0$, then $\eta_{\mathrm{opt}} = \eta_0$; otherwise η_{opt} is between $1/\cos^3\theta_1$ and η_0 and corresponds to the crossing point of the curves $|\dot{\omega}_\eta(r_2)| = \tan\theta_2 - \eta \sin\theta_2$ and $\dot{\omega}_\eta(r_0) = (\eta^{2/3} - 1)^{3/2}$. The ordinate of the crossing point is $\dot{\omega}_{\max}$.

Figure 15 shows plots of η_{opt} and $\dot{\omega}_{\max}$ versus θ_2 for the special case in which $\theta_1 = 0$. Notice that with increasing θ_2 the optimum η rises above 1, first slowly and then rapidly. $\dot{\omega}_{\max}$ also increases from zero at $\theta_2 = 0$ to 10^{-2} at $\theta_2 = 25°$ and to 1 at $\theta_2 = 75°$.

Figure 16 shows plots of $\cos\{2\pi\mathbf{f}[(1 - r^2)^{1/2} + \frac{1}{2}\eta r^2]\}$ versus r in the interval (0, 0.5), corresponding to $\theta_1 = 0$ and $\theta_2 = 30°$. The optimum value $\eta = 1.11395$ is used in Fig. 16(a), and the value $\eta = 1$ is used in Fig. 16(b). The value of $\mathbf{f}$ is 3500 in both plots. Notice how a nonoptimum value of η can increase the oscillations and thereby require a large number of samples for numerical computations.

APPENDIX B

Consider the function

$$\omega_\eta(r) = (1 + r^2)^{1/2} - \tfrac{1}{2}\eta r^2, \qquad r_1 \le r \le r_2, \tag{B1}$$

where $0 \le r_1 \le r_2$ and η is a real parameter. The objective is to find the value of η that minimizes the maximum value of $|\dot{\omega}_\eta(r)|$ in the interval $[r_1, r_2]$. $\dot{\omega}_\eta(r)$ is the derivative of $\omega_\eta(r)$ with respect to r and is given by

$$\dot{\omega}_\eta(r) = (1 + r^{-2})^{-1/2} - \eta r, \qquad r_1 \le r \le r_2. \tag{B2}$$

The second derivative of $w_\eta(r)$ is

$$\ddot{\omega}_\eta(r) = (1 + r^2)^{-3/2} - \eta, \qquad r_1 \le r \le r_2, \tag{B3}$$

which vanishes at

$$r_0 = (\eta^{-2/3} - 1)^{1/2}. \tag{B4}$$

r_0 belongs to $[r_1, r_2]$ provided that

$$(1 + r_2{}^2)^{-3/2} \le \eta \le (1 + r_1{}^2)^{-3/2}. \tag{B5}$$

The value of $\dot{\omega}_\eta(r)$ at r_0 is

$$\dot{\omega}_\eta(r_0) = (1 - \eta^{2/3})^{3/2}. \tag{B6}$$

Let us define θ_1 and θ_2 as follows:

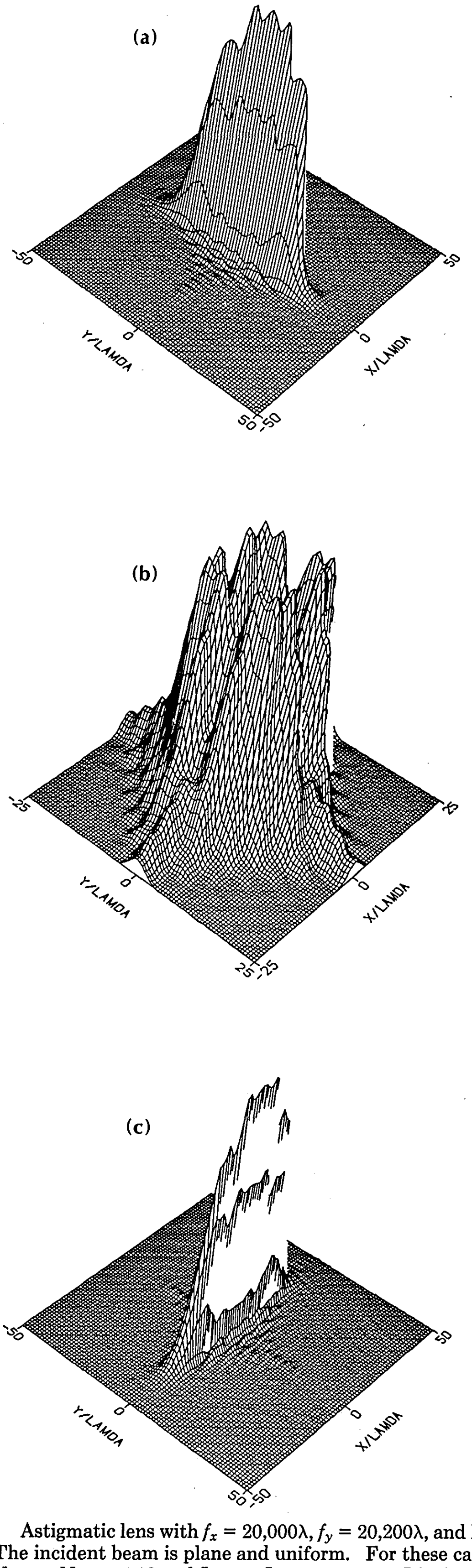

Fig. 12. Astigmatic lens with $f_x = 20{,}000\lambda$, $f_y = 20{,}200\lambda$, and NA = 0.15. The incident beam is plane and uniform. For these calculations, $N_{\max} = N_{\max} = 512$ and $L_{\max} = L_{\max} = 40{,}000$. The intensity pattern is shown at various distances from the lens: (a) **z** = 20,000, (b) **z** = 20,100, and (c) **z** = 20,200.

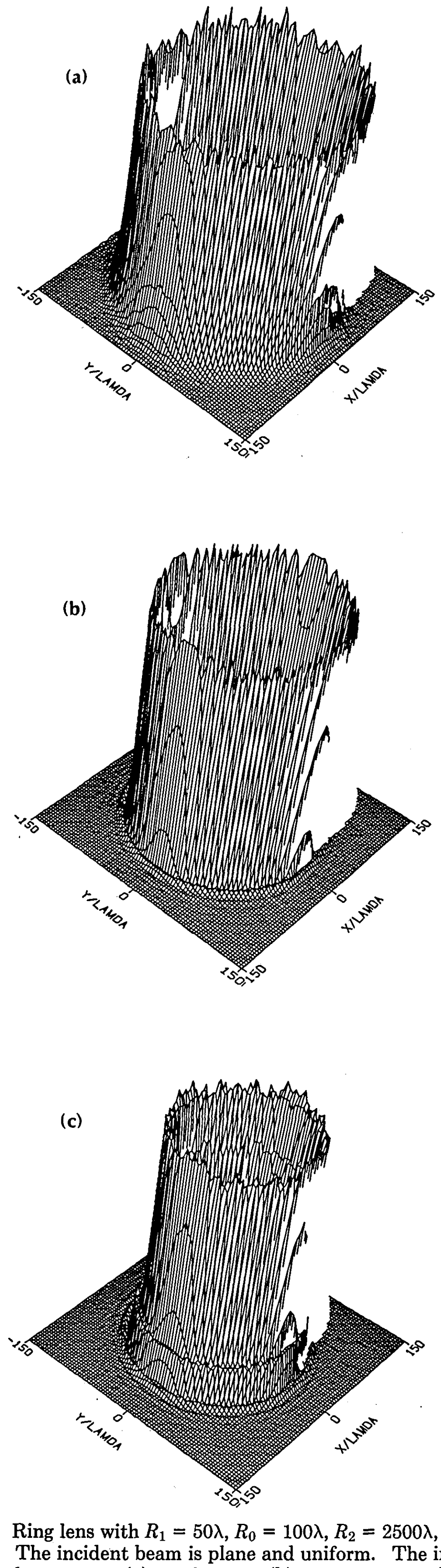

Fig. 13. Ring lens with $R_1 = 50\lambda$, $R_0 = 100\lambda$, $R_2 = 2500\lambda$, and $f = 25{,}000\lambda$. The incident beam is plane and uniform. The intensity patterns shown are at (a) $z = 24{,}750\lambda$, (b) $z = 25{,}000\lambda$, and (c) $z = 25{,}400\lambda$. For these computations $N_{\max} = N_{\max} = 512$ and $L_{\max} = L_{\max} = 25{,}000$.

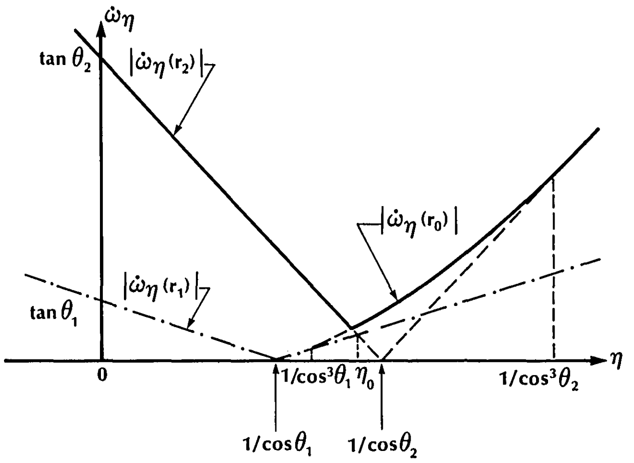

Fig. 14. Various peaks of $|\dot{\omega}_\eta(r)|$ in the interval $[r_1, r_2]$, plotted here as functions of η; the bold curve represents the largest peak. η_{opt} and $\dot{\omega}_{max}$ are the coordinates of the minimum point of the bold curve.

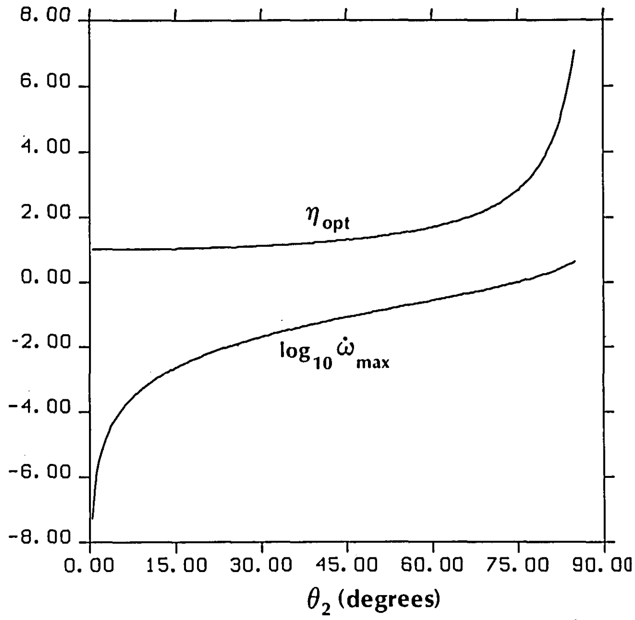

Fig. 15. η_{opt} and $\dot{\omega}_{max}$, as functions of θ_2 for $\theta_1 = 0$. Note that the scale for $\dot{\omega}_{max}$ is logarithmic. The particular value of θ_1 chosen here corresponds to $r_1 = 0$, while $r_2 = \sin\theta_2$.

$$\tan\theta_1 = r_1,$$

$$\tan\theta_2 = r_2; \tag{B7}$$

then the values of $\dot{\omega}_\eta(r)$ at r_1 and r_2 are

$$\dot{\omega}_\eta(r_1) = -\eta\tan\theta_1 + \sin\theta_1, \tag{B8}$$

$$\dot{\omega}_\eta(r_2) = -\eta\tan\theta_2 + \sin\theta_2. \tag{B9}$$

The maximum of $|\dot{\omega}_\eta(r)|$ over $[r_1, r_2]$, which will be referred to as $\dot{\omega}_{max}$, is at r_1 or at r_2 or, in case r_0 happens to be within the interval, at r_0. Thus, among Eqs. (B6), (B8), and (B9), one equation represents the maximum absolute value of the function. Figure 17 shows a plot of these three functions versus η. Note that according to relation (B5) the range of η over which r_0 lies between r_1 and r_2 is

$$\cos^3\theta_2 \le \eta \le \cos^3\theta_1. \tag{B10}$$

The functions $\dot{\omega}_\eta(r_1)$ and $-\dot{\omega}_\eta(r_2)$ cross at η_0, where

$$\eta_0 = \frac{\sin\theta_1 + \sin\theta_2}{\tan\theta_1 + \tan\theta_2}. \tag{B11}$$

If $\cos^3\theta_1 \le \eta_0$, then $\eta_{opt} = \eta_0$; otherwise η_{opt} is between η_0 and $\cos^3\theta_1$ and corresponds to the crossing point of the curves $|\dot{\omega}_\eta(r_2)| = \eta\tan\theta_2 - \sin\theta_2$ and $\dot{\omega}_\eta(r_0) = (1 - \eta^{2/3})^{3/2}$. The ordinate of the crossing point is $\dot{\omega}_{max}$.

Notice that η_{opt} as obtained in Appendix A is the inverse of η_{opt} in this Appendix, provided that the corresponding θ's are identical. Of course, when θ_1 (or θ_2) in one problem is equal to

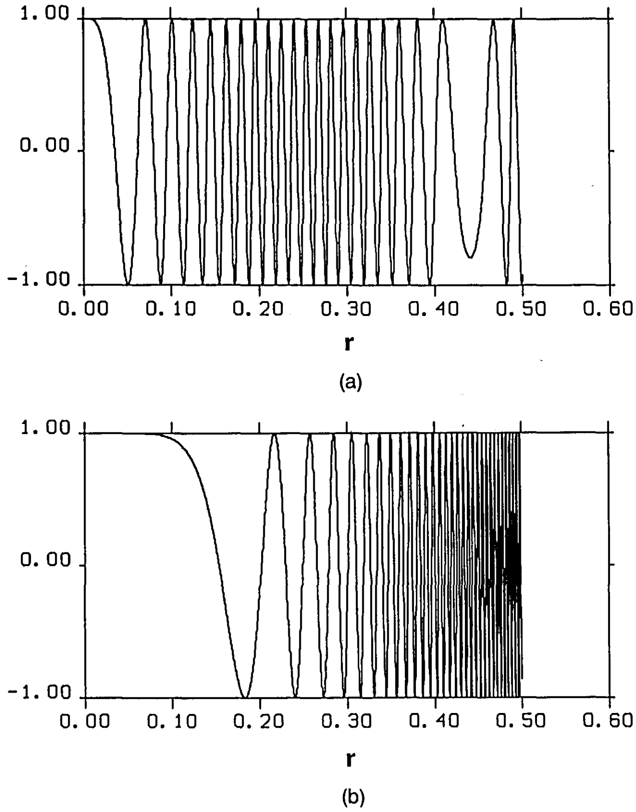

Fig. 16. Two plots of $\cos\{2\pi\mathbf{f}[(1 - r^2)^{1/2} + \frac{1}{2}\eta r^2]\}$ versus r. In (a) the optimum value of $\eta = 1.11395$ is used, whereas in (b) $\eta = 1$ is used. In both cases $\mathbf{f} = 3500$, $r_1 = 0$, and $r_2 = 0.5$.

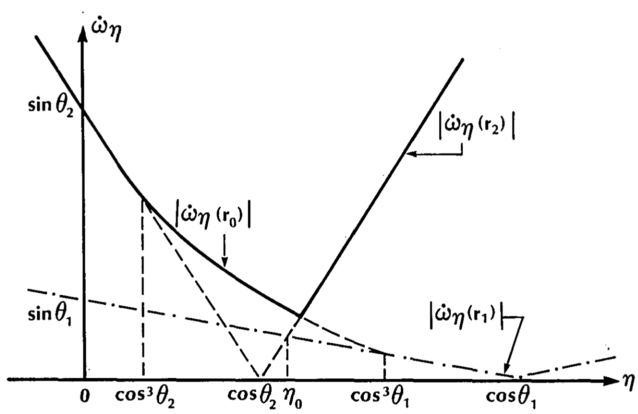

Fig. 17. Various peaks of $|\dot{\omega}_\eta(r)|$ in the interval $[r_1, r_2]$, plotted here as functions of η; the bold curve represents the largest peak. η_{opt} and $\dot{\omega}_{max}$ are the coordinates of the minimum point of the bold curve.

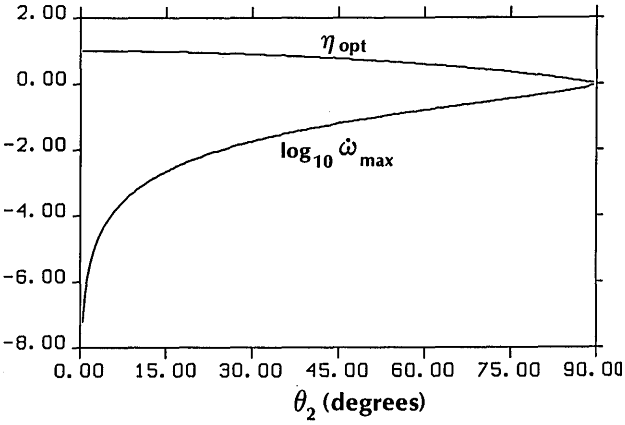

Fig. 18. η_{opt} and $\dot{\omega}_{max}$ as functions of θ_2 for $\theta_1 = 0$. Note that the scale for $\dot{\omega}_{max}$ is logarithmic. The particular value of θ_1 chosen here corresponds to $r_1 = 0$, while $r_2 = \tan\theta_2$.

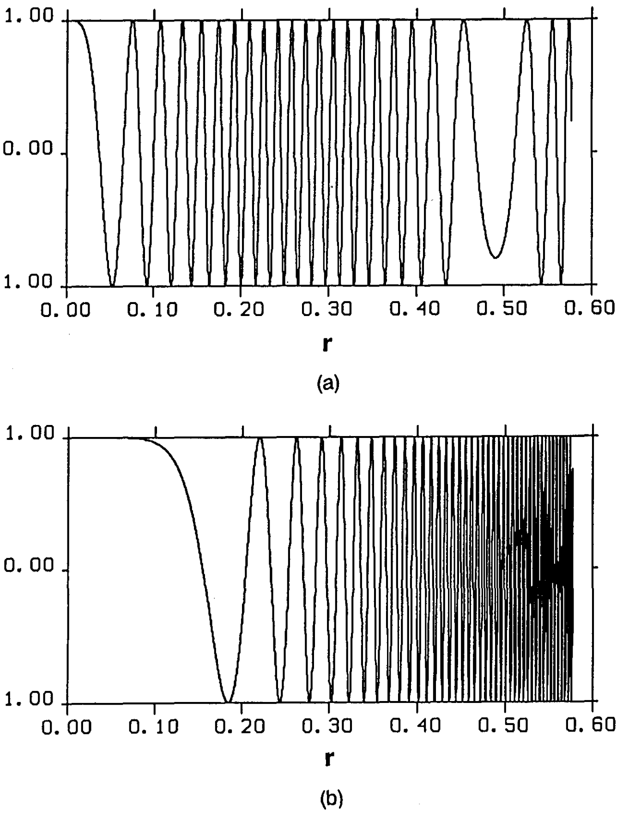

Fig. 19. Two plots of $\cos\{2\pi\mathbf{f}[(1 + r^2)^{1/2} - \frac{1}{2}\eta r^2]\}$ versus r. In (a) the optimum value of $\eta = 0.8977$ is used, whereas in (b) $\eta = 1$ is used. In both cases $\mathbf{f} = 3500$, $r_1 = 0$, and $r_2 = 0.577$.

θ_1 (or θ_2) in the other, the r_1 (or r_2) values for the two problems are not equal, as can be observed by comparing Eqs. (A7) and (B7). When the corresponding θ's are identical, we have

$$\dot{\omega}_{max}{}^{(A)} = \tan\theta_2 - \eta_{opt}{}^{(A)} \sin\theta_2, \tag{B12}$$

$$\dot{\omega}_{max}{}^{(B)} = \eta_{opt}{}^{(B)} \tan\theta_2 - \sin\theta_2. \tag{B13}$$

Also, $\eta_{opt}{}^{(A)} = 1/\eta_{opt}{}^{(B)}$; therefore

$$\dot{\omega}_{max}{}^{(A)}/\eta_{opt}{}^{(A)} = \dot{\omega}_{max}{}^{(B)}, \tag{B14}$$

$$\dot{\omega}_{max}{}^{(B)}/\eta_{opt}{}^{(B)} = \dot{\omega}_{max}{}^{(A)}. \tag{B15}$$

Figure 18 shows plots of η_{opt} and $\dot{\omega}_{max}$ versus θ_2 for the special case in which $\theta_1 = 0$. Notice that with increasing θ_2 the optimum η drops below 1, while $\dot{\omega}_{max}$ rises rapidly from 0 at the origin to 10^{-2} at $\theta_2 = 25°$ and to 1 at $\theta_2 = 90°$.

Figure 19 shows plots of $\cos\{2\pi\mathbf{f}[(1 + r^2)^{1/2} - \frac{1}{2}\eta r^2]\}$ versus r in the interval [0, 0.577] corresponding to $\theta_1 = 0$ and $\theta_2 = 30°$. The value $\mathbf{f} = 3500$ is used in these plots. In Fig. 19(a) the optimum value $\eta = 0.8977$ is used, and the value $\eta = 1$ is used in Fig. 19(b). Notice how a nonoptimum η increases the oscillations and thereby requires a large number of samples for numerical computations.

APPENDIX C

Consider the function

$$\omega_\eta(r) = [1 + (r - R)^2]^{1/2} - \tfrac{1}{2}\eta r^2, \tag{C1}$$

where r is in the interval $[r_1, r_2]$ with $0 \le r_1 \le R \le r_2$. R is a constant, and η is a real parameter. The objective is to find the value of η that minimizes the maximum value of $|\dot{\omega}_\eta(r)|$ in the interval $[r_1, r_2]$. $\dot{\omega}_\eta(r)$ is the derivative of $\omega_\eta(r)$ with respect to r and is given by

$$\dot{\omega}_\eta(r) = (r - R)[1 + (r - R)^2]^{-1/2} - \eta r, \qquad r_1 \le r \le r_2. \tag{C2}$$

The second derivative of $\omega_\eta(r)$ is

$$\ddot{\omega}_\eta(r) = [1 + (r - R)^2]^{-3/2} - \eta, \qquad r_1 \le r \le r_2, \tag{C3}$$

which vanishes at the following two points:

$$r_0^{\pm} = R \pm (\eta^{-2/3} - 1)^{1/2}. \tag{C4}$$

These points will be in $[r_1, r_2]$, provided that

$$[1 + (r_2 - R)^2]^{-3/2} \le \eta \le 1, \tag{C5a}$$

$$[1 + (R - r_1)^2]^{-3/2} \le \eta \le 1. \tag{C5b}$$

The values of $\dot{\omega}_\eta(r)$ at $r_0^{\pm}$ are

$$\dot{\omega}_\eta(r_0^{\pm}) = \pm(1 - \eta^{2/3})^{3/2} - \eta R. \tag{C6}$$

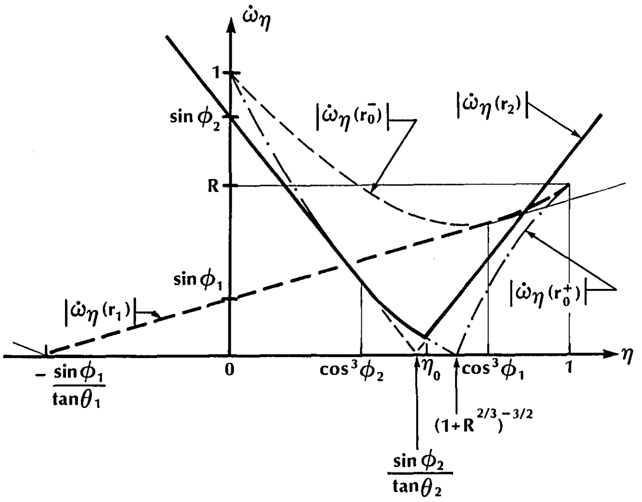

Fig. 20. Various peaks of $|\dot{\omega}_\eta(r)|$ in the interval $[r_1, r_2]$, plotted here as functions of η. The bold solid curve represents the largest peak to the right of R, whereas the bold dashed curve corresponds to the largest peak to the left of R. The larger of the two curves at any η thus gives the largest peak, and the optimum η is the point at which the largest peak is minimum.

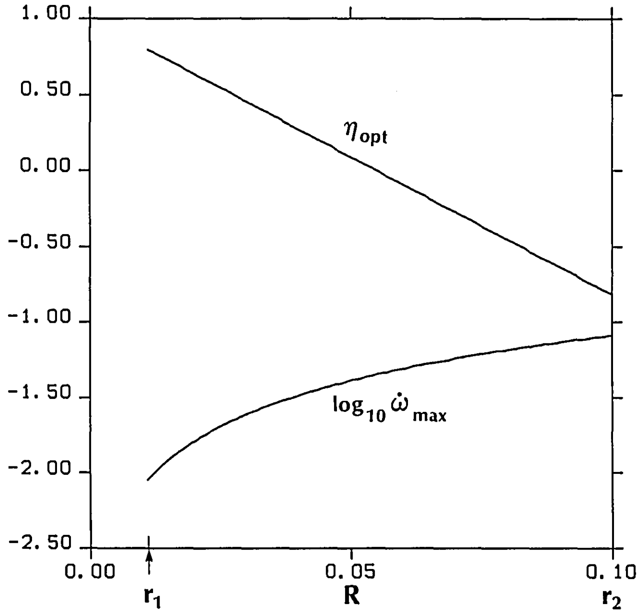

Fig. 21. η_{opt} and $\dot{\omega}_{max}$ as functions of R for $r_1 = 0.01$ and $r_2 = 0.1$. Note that the scale for $\dot{\omega}_{max}$ is logarithmic.

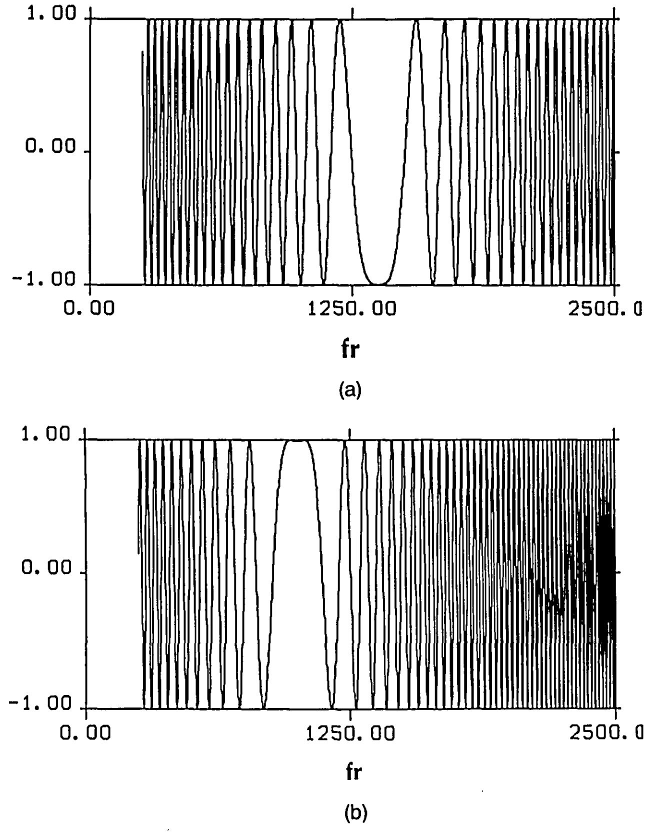

Fig. 22. Two plots of $\cos(2\pi\mathbf{f}\{[1 + (r - R)^2]^{1/2} - \tfrac{1}{2}\eta r^2\})$ versus **f**r. In (a) the optimum value of $\eta = 0.272$ is used, whereas in (b) $\eta = 0$ is used. In both cases $\mathbf{f} = 25000$, $r_1 = 0.01$, and $r_2 = 0.1$.

Let us define θ_1, ϕ_1, θ_2, and ϕ_2 as follows:

$$\tan\theta_1 = r_1, \tag{C7a}$$

$$\tan\theta_2 = r_2, \tag{C7b}$$

$$\tan\phi_1 = R - r_1, \tag{C7c}$$

$$\tan\phi_2 = r_2 - R; \tag{C7d}$$

then the values of $\dot{\omega}_\eta(r)$ at r_1 and r_2 are

$$\dot{\omega}_\eta(r_1) = -\sin\phi_1 - \eta\tan\theta_1, \tag{C8}$$

$$\dot{\omega}_\eta(r_2) = \sin\phi_2 - \eta\tan\theta_2. \tag{C9}$$

The maximum of $|\dot{\omega}_\eta(r)|$ over $[r_1, r_2]$, which will be referred to as $\dot{\omega}_{max}$, is at r_1 or r_2 or, in case r_0^+ or r_0^- happens to be within the interval, at r_0^+ or r_0^-. Thus, among Eqs. (C6), (C8), and (C9), one equation represents the maximum absolute value of the function. Figure 20 shows a plot of these four functions versus η. Note that according to relations (C5) the ranges of η over which $r_0^\pm$ fall between r_1 and r_2 are

$$\cos^3\phi_2 \le \eta \le 1 \qquad (\text{for } r_0^+), \tag{C10a}$$

$$\cos^3\phi_1 \le \eta \le 1 \qquad (\text{for } r_0^-). \tag{C10b}$$

In Fig. 20 we have constructed two functions. The first, shown as a dark solid curve, represents the maximum of $|\dot{\omega}_\eta(r)|$ to the right of R and is the larger of the two functions $|\dot{\omega}_\eta(r_2)|$ and $|\dot{\omega}_\eta(r_0^+)|$ when the latter is in the region of relation (C10a). Evidently, there is no contribution to this curve from $|\dot{\omega}_\eta(r_0^+)|$ unless

$$\cos^3\phi_2 < \frac{\sin\phi_2}{\tan\theta_2}. \tag{C11}$$

The section of $|\dot{\omega}_\eta(r_0^+)|$ that is used here is between $\cos^3\phi_2$ and η_0, where η_0 belongs to the interval $[\sin\phi_2/\tan\theta_2, (1 + R^{2/3})^{-3/2}]$ and represents the crossing point of the curves for $|\dot{\omega}_\eta(r_2)| = \eta\tan\theta_2 - \sin\phi_2$ and $\dot{\omega}_\eta(r_0^+) = (1 - \eta^{2/3})^{3/2} - \eta R$. The second function, shown as a bold dashed curve, consists of $|\dot{\omega}_\eta(r_1)|$ when $\eta \le \cos^3\phi_1$ and of $|\dot{\omega}_\eta(r_0^-)|$ when $\eta \ge \cos^3\phi_1$. This function represents the largest value of $|\dot{\omega}_\eta(r)|$ when r is to the left of R. Thus we need to investigate the larger of the above two functions. Two possibilities exist:

1. $\sin\phi_1 > \sin\phi_2$. In this case η_{opt} is negative and is given by

$$\eta_{opt} = \frac{\sin\phi_2 - \sin\phi_1}{\tan\theta_2 + \tan\theta_1}. \tag{C12}$$

2. $\sin\phi_1 < \sin\phi_2$. In this case the optimum η is at the crossing of the two dark curves. The ordinate of the crossing point is $\dot{\omega}_{max}$.

Figure 21 shows plots of η_{opt} and $\dot{\omega}_{max}$ versus R for $r_1 = 0.01$ and $r_2 = 0.1$. When R is halfway between r_1 and r_2, $\eta_{opt} = 0$ and the high-frequency terms cannot be factored out. As R moves closer to r_1, however, $\dot{\omega}_{max}$ drops rapidly and η_{opt} increases toward 1.

Figure 22 shows plots of $\cos(2\pi\mathbf{f}\{[1 + (r - R)^2]^{1/2} - \tfrac{1}{2}\eta r^2\})$ versus **f**r for $\mathbf{f} = 25{,}000$, $\mathbf{f}r_1 = 250$, $\mathbf{f}r_2 = 2500$, and $\mathbf{f}R = 1000$. In Fig. 22(a) the optimum value $\eta = 0.272$ is used, and in Fig. 22(b), $\eta = 0$ is used. Note how optimum η can balance the oscillations at the two extremes of the aperture and consequently can minimize the required number of samples for numerical computations.

ACKNOWLEDGMENT

This study has been supported by a grant from the IBM Corporation.

REFERENCES

1. E. Wolf, "Electromagnetic diffraction in optical systems: an integral representation of the image field," Proc. R. Soc. Ser. A **253,** 349–357 (1959).
2. B. Richards and E. Wolf, "Electromagnetic diffraction in optical systems: structure of the image field in an aplanatic system," Proc. R. Soc. Ser. A **253,** 358–379 (1959).
3. D. R. Rhodes, "On the stored energy of planar apertures," IEEE Trans. Antennas Propag. **AP-14,** 676–683 (1966).
4. G. Borgiotti, "Fourier transforms method of aperture antennas problem," Alta Frequenza **32,** 196–204 (1963).
5. M. Born and E. Wolf, *Principles of Optics*, 6th ed. (Pergamon, Oxford, 1980).
6. K. Miyamoto and E. Wolf, "Generalization of the Maggi–Rubinowitz theory of the boundary diffraction wave—part I," J. Opt. Soc. Am. **52,** 615–625 (1962).
7. G. W. Farnell, "Measured phase distribution in the image space of a microwave lens," Can. J. Phys. **36,** 935–943 (1958).
8. Y. Li and E. Wolf, "Three-dimensional intensity distribution near the focus in systems of different Fresnel numbers," J. Opt. Soc. Am. A **1,** 801–808 (1984).
9. V. N. Mahajan, "Axial irradiance and optimum focusing of laser beams," Appl. Opt. **22,** 3042–3053 (1983).
10. M. Mansuripur, "Distribution of light at and near the focus of high-numerical-aperture objectives," J. Opt. Soc. Am. A **3,** 2086–2093 (1986).
11. J. W. Goodman, *Introduction to Fourier Optics* (McGraw-Hill, New York, 1968).
12. M. Mansuripur and C. Pons, "Diffraction modeling of optical path for magneto-optical disk systems," in *Optical Storage Technology and Applications*, D. Carlin, Y. Tsunoda, and A. Jamberdino, eds., Proc. Soc. Photo-Opt. Instrum. Eng. **899,** 56–60 (1988).
13. F. Jenkins and H. White, *Fundamentals of Physical Optics*, 1st ed. (McGraw-Hill, New York, 1937).